*Review*

# Cobalt Sulfide (Co$_9$S$_8$)-Based Materials with Different Dimensions: Properties, Preparation and Applications in Photo/Electric Catalysis and Energy Storage

**Chuantao Wang, Xiangxiang Pang** (ID)**, Guangqing Wang, Loujun Gao * and Feng Fu ***

Shaanxi Key Laboratory of Chemical Reaction Engineering, Research Institute of Comprehensive Energy Industry Technology, College of Chemistry & Chemical Engineering, Yan'an University, Yan'an 716000, China
* Correspondence: glj@yau.edu.cn (L.G.); yadxfufeng@126.com (F.F.)

**Abstract:** Due to their excellent properties and unique structures, transition metal sulfides play an important role in the development of efficient and stable photoelectric catalysts. In recent years, their potential applications have expanded from photoelectric catalysis to energy storage, especially as materials for key components of electrochemical energy storage. As a typical multifunctional metal sulfide catalyst, Co$_9$S$_8$ is highly attractive due to its high conductivity, better stability, suitable band structure, enhanced performance and wide applications. A large number of studies have shown that strategically modified Co$_9$S$_8$-based materials have greater advantages in various applications compared with pure Co$_9$S$_8$. Therefore, this review will evaluate the physicochemical properties and the preparation of different dimensions of Co$_9$S$_8$-based materials, and the influence of different structures on the photoelectrochemical energy of materials will be described. In addition, the research progress regarding the evolution of hydrogen photocatalytic, electrocatalytic water splitting and various electrochemical energy storage materials will be emphasized. Finally, the challenges faced by Co$_9$S$_8$-based materials and the research directions for their future applications will be discussed.

**Keywords:** Co$_9$S$_8$-based materials; dimensions; energy storage; HER

## 1. Introduction

The need for large-scale production of renewable energy is driven by the depletion of fossil fuels and serious environmental pollution problems [1–3]. Efficient and environmentally friendly photoelectric catalytic technology has been widely used in energy conversion. However, there are still some problems to be solved, such as the recombination of carriers and the slow kinetics of electrocatalytic reactions, which hinder the further development of photoelectric catalytic technology. Therefore, it is necessary to explore excellent photoelectric catalysts to improve the reaction efficiency.

Metal sulfide (MSx) is considered to be one of the most important materials for the preparation of highly photoelectrochemical active materials, owing to its high stability and excellent redox properties [4–6]. As a typical cobalt-rich sulfide, Co$_9$S$_8$ has high conductivity, good stability and a relatively narrow band gap. Meanwhile, Co$_9$S$_8$ shows great diversity in size, structure and performance when used by photoelectric catalysts and by various materials for energy storage. In order to obtain more active sites and better performance, Co$_9$S$_8$ modification strategies are usually implemented, including morphology control, heterostructure construction, defect engineering, etc. [7–9]. For example, Zhao first developed a hierarchical Co$_9$S$_8$@ZnAgInS heterostructure cage to achieve efficient photocatalytic hydrogen production. Li used the doping strategy to prepare an efficient all-pH electrocatalyst Co$_9$S$_8$/nitrogen-doped carbo@MoS$_2$. The Co$_9$S$_8$-based materials after modification have a controllable high specific surface area and a reasonable pore size distribution, which is conducive to the exposure of the active site, and has made an outstanding

contribution to electrocatalytic water splitting and photoelectric catalysis hydrogen evolution. In addition, as a key material for energy storage, $Co_9S_8$-based materials have been proven to improve the coulomb efficiency and cycle life of batteries, and can also provide rich surface functional groups for Faraday reactions of supercapacitors.

In this review, we first briefly introduce the physicochemical properties of $Co_9S_8$. Subsequently, the preparation of different dimensions and applications of $Co_9S_8$-based materials in photoelectric catalysis hydrogen evolution, electrocatalytic water splitting and various means of electrochemical energy storage are discussed (Figure 1). This study will provide prospects for the development of $Co_9S_8$-based materials as photoelectric catalysts and new-generation energy storage materials in the future.
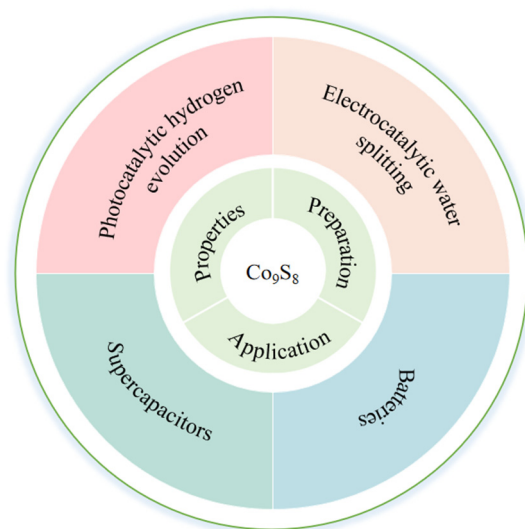


**Figure 1.** Properties, preparation and application (photocatalytic hydrogen evolution, electrocatalytic water splitting, batteries and supercapacitors) of $Co_9S_8$-based materials.

## 2. Properties

$Co_9S_8$ nanomaterials have attracted attention from various fields due to their distinct structures and surface areas, thus exhibiting excellent physical and chemical properties. Magnetism, the most fundamental property of $Co_9S_8$, is profoundly affected by the temperature of the reaction system. For example, Robert F. Heidelberg summarized and described the susceptibility of cobalt–sulfur systems, which mentioned that $Co_9S_8$ is antiferromagnetic when the Néel temperature is higher than the decomposition temperature [10]. Erika Dutková and colleagues studied the magnetic properties of $Co_9S_8$ nanoparticles synthesized by mechanical chemistry using a Superconducting Quantum Interference Device (SQUID) magnetometer. The room-temperature magnetic data supports the paramagnetic spin structure of the nanoparticle, and the temperature dependence of the magnetization at low temperatures suggests a transition from paramagnetism to weak ferromagnetism or ferromagnetism [11]. In addition, Zhou and colleagues also studied the magnetic properties of $Co_9S_8$ hollow microspheres successfully prepared and reached the same conclusion [12]. Therefore, the study of the magnetic properties of $Co_9S_8$ confirms the potential application of $Co_9S_8$ in magnetic fields.

A large number of metallic sulfides have outstanding electrical conductivity, such as $Co_9S_8$ and $Ni_3S_2$, but magnetic instability and electron interactions make them of insignificant importance [13]. To play metallic sulfides' crucial role, the most common approach is to increase the number of free carriers by introducing different dopants, and an increase in the doping concentration leads to an increase in the conductance [14]. It is worth noting that $Co_9S_8$ also has rich redox properties, which contributes to the generation of active sites for chemical reactions, especially electrocatalytic hydrogen evolution reaction

(HER) and oxygen evolution reaction (OER), which also plays an important role in the further application of $Co_9S_8$ in the field of photoelectric catalysis [15].

## 3. Different Dimensions of $Co_9S_8$-Based Materials

Pokropivny and Skorokhod proposed a classification scheme for nanostructured materials (NSMs) in 2007, namely zero-dimensional (0D), one-dimensional (1D), two-dimensional (2D) and three-dimensional (3D) [16]. It is noteworthy that the physical, chemical and electronic properties of nanomaterials with different dimensions could be quite different from one another, which is attributed to the fact that the intensity of electron motion increases with the increase of dimension [17]. So far, many technologies have been developed for controllable preparation of 0D–3D $Co_9S_8$ nanomaterials, and 0D nanoparticles, 1D nanotubes, nanorods, nanowires and needles, 2D nanosheets, nanoplates, nanolayers and nanowalls, 3D hollow spheres and flower-like structures have been obtained. Therefore, based on the above classification, this section discusses the structure and preparation method of $Co_9S_8$ nanomaterials from 0D–3D.

### 3.1. Zero-Dimensional (0D) Structure

In recent years, the great potential of 0D-nanostructured materials in photoelectric catalysis, solar cells and lithium ion batteries has promoted the synthesis of 0D-structured $Co_9S_8$-based materials. Feng prepared carbon-coated $Co_9S_8$ nanoparticles ($Co_9S_8$@C) from a mixture of cobalt nitrate and trithiocyanuric acid by direct heat treatment in $N_2$ atmosphere at 700 °C. It is noteworthy that trithiocyanuric acid is both a sulfur and a carbon source in this reaction system [18]. Wang also produced well-coated $Co_9S_8$@C nanomaterials using the vulcanization method (Figure 2a) [19]. Furthermore, unlike the above, Liu prepared $Co_9S_8$@C ultrafine nanomaterials using sucrose as the carbon source and using solid state reaction and mechanical ball milling (Figure 2b). It is certain that ball milling is not only a process of particle size reduction, but also promotes more effective binding between carbon and $Co_9S_8$ [20]. Lu synthesized carbon-decorated and graphene-fixed amorphous $Co_9S_8$ hollow nanoparticles using a "thermal injection" method [21]. A large number of experimental studies have shown that wrapping unique structurally modified nanoparticles in a doped mesoporous network with more active sites is an effective way to obtain ideal materials with high activity. Zhang, Luo, Du and Wang have reported that metal-organic framework (MOFs)-derived $Co_9S_8$ nanoparticles embedded in nitrogen and sulfur co-doped carbon composites show excellent performance [22–25]. Using inorganic salt as a template, Yu prepared a series of $Co_9S_8$ nanoparticles embedded with N and S co-doped carbon through three steps of grinding, carbonation and acid leaching (Figure 2c). It is suggested that the ratio of precursor, annealing temperature and the type of salt can adjust the porosity, heteroatomic content and crystal structure of the product [26–28]. Different synthesis methods have different advantages. Zhang used carbon dots (CDs) to prepare $Co_9S_8$ nanoparticles in N and S co-doped carbon materials. CDs distributed uniformly in the matrix of $Co_9S_8$ nanoparticles and played a key role in improving specific surface area and electrical conductivity (Figure 2d) [29]. Wang grew monodispersed $Co_9S_8$ nanoparticles with a particle size of about 8 nm due to the restriction of organic ligand oleamine on the surface of Reduced Graphene Oxide (RGO) by a simple thermal injection method [30]. Li prepared hollow carbon nanotubes with single cobalt atoms integrated with $Co_9S_8$ nanoparticles. The structure of the material was verified by X-ray absorption spectroscopy and aberration-corrected scanning transmission electron microscopy [31]. Zhang reported a mild ion exchange method for the preparation of carbon nanofibers modified with $Co_9S_8$ nanoparticles. Specifically, $Co_9S_8$ nanoparticles were converted from cobalt oxide precursor nanoparticles in a microwave hydrothermal process and then modified on the carbon nanofiber skeleton. The composition of nanofibers can be adjusted by changing the content of cobalt acetate in the precursor. In terms of materials, $Co_9S_8$ nanoparticles with favorable dispersion act as redox centers for energy storage, while porous carbon nanofibers provide fast electron transfer pathways [32].
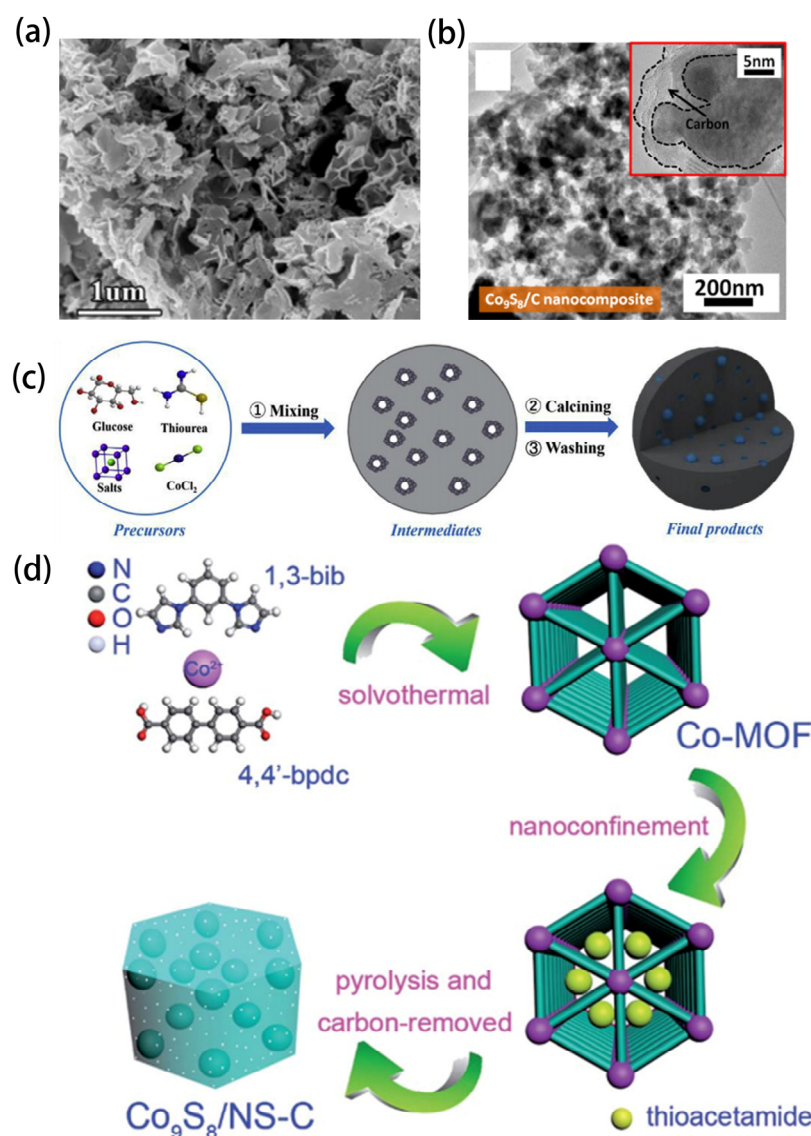
**Figure 2.** (**a**) SEM images of $Co_9S_8$/C-T precursor. Reprinted with permission from Reference [19]. Copyright (2018) Elsevier Ltd. All rights reserved. (**b**) TEM images of $Co_9S_8$/C Nanocomposite. Reprinted with permission from Reference [20]. Copyright (2018) Springer Ltd. All rights reserved. (**c**) The synthetic strategy of the alkali metal doped $Co_9S_8$ NPs embedded, N, S co-doped carbons. Reprinted with permission from Reference [26]. Copyright (2020) Elsevier Ltd. All rights reserved. (**d**) The synthesis process of $Co_9S_8$/NS-C. Reprinted with permission from Reference [29]. Copyright (2017) Royal Society of Chemistry.

### 3.2. One-Dimensional (1D) Structure

Recently reported 1D $Co_9S_8$-based nanomaterials can be divided into nanowires, nanotubes and nanorods according to their morphology. The application of nanowire in an energy storage system is beneficial to the strong contact area between electrode and electrolyte. In addition, the high electrochemical activity is due to the abundance of active sites, rapid electron transport and gas release. Yang grew $Co_9S_8$ nanowires on carbon fiber paper by using a hydrothermal method (Figure 3a). Notably, $Co_9S_8$ nanowires were encapsulated in a fluffiness shell consisting of a continuous N, S co-doped carbon coating decorated with abundant vertically growing N, co-doped carbon nanotube materials. The material not only provides excellent voids for rapid mass transfer, but also provides a large specific surface area for loading of active sites [33]. Dong constructed a one-dimensional cobalt sulfide and vanadium sulfide heterojunction nanowire bi-functional electrocatalyst grown on carbon

cloth (Figure 3b). The 1D linear $Co_9S_8$-$V_3S_4$ heterojunction has strong electron coupling, which is favorable for hydrogen evolution reaction [34]. Similar to nanowire, nanotubes and nanorods have attracted the attention of researchers because of their extreme specific surface area. Liu obtained a core-shell nanotube array with rich oxygen vacancy $Co_9S_8$@NiCo-LDH (Figure 3c). In situ growth and electrodeposition of flexible carbon cloth carrier were used [35]. Similarly, Zhu successfully fabricated $Co_9S_8$@Ni(OH)$_2$ core-shell nanotube arrays with very large specific surface area by electrodeposition (Figure 3d) [36]. Zhang and Li assembled one-dimensional $Co_9S_8$ nanotubes and two-dimensional nanosheets to prepare materials with excellent synergistic properties (Figure 3e) [37,38]. Wu synthesized a novel hybrid material of Molybdenum sulfide laminate modified by $Co_9S_8$ nanotubes through continuous solvent heat treatment. X-ray diffraction, field emission scanning electron microscopy, transmission electron microscopy and other techniques were used to characterize the material, which not only proved that the decoration was amorphous $MoS_x$, but also showed that there was a strong interface interaction between the two phases [39]. Du successfully synthesized a series of $Co_9S_8$ nanorod arrays with dual-function electrocatalysts doped with Mo on nickel foam for the first time by using a hydrothermal sulfidation process (Figure 3f) [40]. In addition, Du reported an in situ deposition method for adjusting the Ni(OH)$_2$ loading capacity on a $Co_9S_8$ surface by adjusting the number of deposition cycles (Figure 3g,h). As a perfect carrier, one-dimensional $Co_9S_8$ nanorods enhanced the uniform dispersion of amorphous Ni(OH)$_2$ nanoparticles. The electrolytic deposition of amorphous Ni(OH)$_2$ nanoparticles coated on the surface of $Co_9S_8$ nanorods greatly improved the interface effect and provided a more effective active center for the water splitting reaction [41].
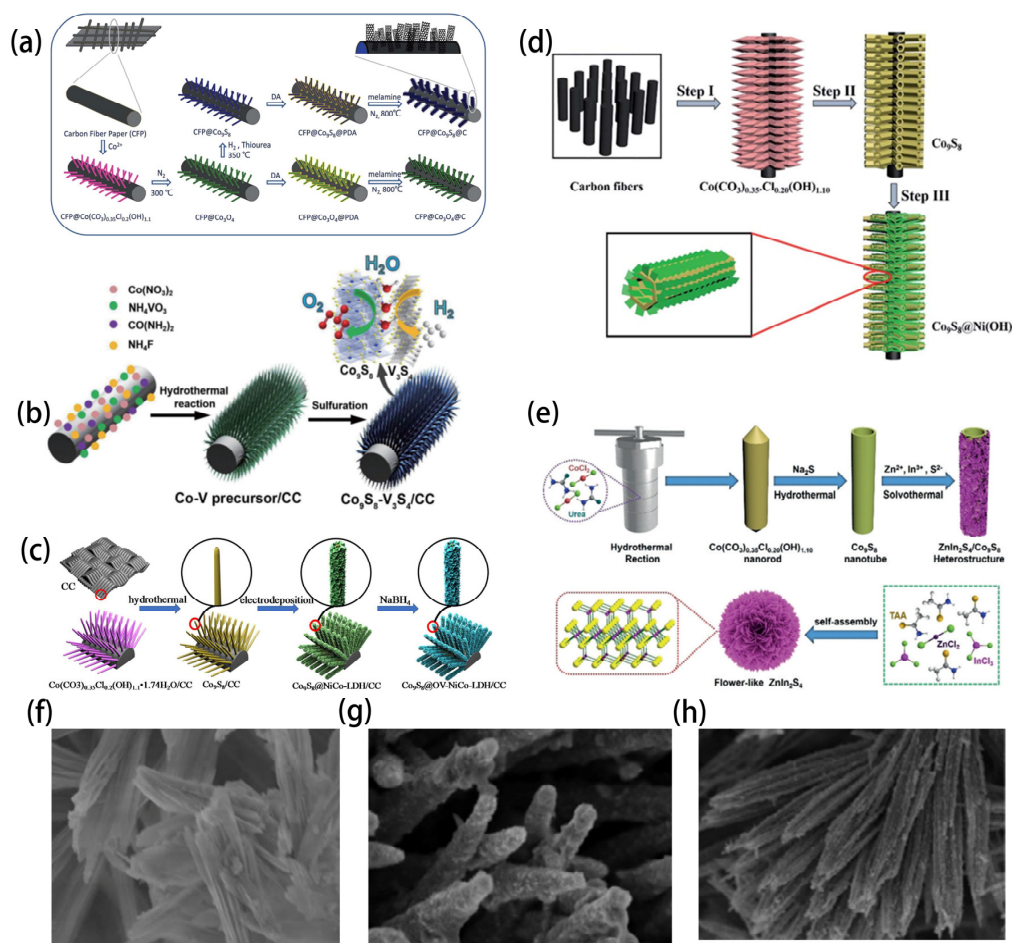


**Figure 3.** (**a**) The synthetic process for CFP supported $Co_9S_8$@N,S-codoped carbon nanowires with surfaces. Reprinted with permission from Reference [33]. Copyright (2018) Royal Society of Chemistry.

(**b**) Schematic diagram of the synthesis of 1D $Co_9S_8$-$V_3S_4$/CC nanowires. Reprinted with permission from Reference [34]. Copyright (2021) Springer Ltd. All rights reserved. (**c**) Schematic diagram of the detailed synthesis process of $Co_9S_8$@OV-NiCo-LDH core-shell nanotube arrays. Reprinted with permission from Reference [35]. Copyright (2022) Elsevier Ltd. All rights reserved. (**d**) Schematic fabrication process of $Co_9S_8$@Ni(OH)$_2$ core–shell NT arrays on CFs. Reprinted with permission from Reference [36]. Copyright (2017) Royal Society of Chemistry. (**e**) Illustration of the fabrication process of hierarchical $Co_9S_8$/$ZnIn_2S_4$ tubular photocatalyst. Reprinted with permission from Reference [37]. Copyright (2020) Wiley-VCH. (**f**) SEM of $Co_9S_8$-3. Reprinted with permission from Reference [40]. Copyright (2019) Elsevier Ltd. All rights reserved. (**g**,**h**) SEM of $Co_9S_8$/NF. Reprinted with permission from Reference [41]. Copyright (2019) Elsevier Ltd. All rights reserved.

### 3.3. Two-Dimensional (2D) Structure

This section demonstrates the preparation of various 2D nanoplates and nanosheets made from $Co_9S_8$-based nanomaterials. Due to its elevated surface volume ratio, nanometer thickness and fascinating electrocatalytic activity, $Co_9S_8$ is considered as an ideal material for electrocatalysts. By changing the filling coefficient, Yang and colleagues synthesized cobalt sulfide precursors with different morphs by hydrothermal method and obtained ultra-thin $Co_9S_8$ nanosheets under the condition that the filling rate of hot autoclaves reached 60% (Figure 4a) [42]. Li successfully designed and synthesized dual-function electrocatalyst $Co_9S_8$/C nanosheets by reducing $Co_3O_4$/CNS precursor with sodium sulfide (Figure 4b) [43]. One of the benefits of using 2D materials is that such composites can easily interact and combine with other materials of different dimensions. For example, Zhang designed a novel two-dimensional hexagonal $WS_2$-sided $Co_9S_8$ heterostructure nanosheet structure on the surface of a carbon nanofiber skeleton [44]. Xing reported and characterized, in detail, layered $Co_3O_4$@$Co_9S_8$ nanowalls assembled from numerous nanosheets [45]. The material with a large number of defects can induce positive effects on the atoms in the ultrathin two-dimensional structure to improving its intrinsic activity, which is beneficial to improve the excellent properties of the material. Wang and colleagues first synthesized porous 2D $Co_9S_8$ nanosheets rich in defects and applied them to the cathode of Li-$O_2$ batteries (Figure 4c). It is worth mentioning that the two-dimensional structure and in-plane holes of the catalyst not only facilitate mass transfer, but also provide active sites for sulfur-rich substances [46]. In addition, using cobalt dibutyl dithiocarbamate as raw material, Zhang and colleagues prepared defective $Co_9S_8$-based ultrathin nanosheets by direct pyrolysis in organic amine solvent [47]. Doping is a particularly popular method to improve material properties. Both Wang and Li successfully synthesized two-dimensional $Co_9S_8$ nanosheets uniformly distributed on the surface of two-dimensional N-doped graphene [48,49]. Li reported a sandwich structure in which $Co_9S_8$ is confined between the graphene scaffold folding layer and the N-carbon layer (Figure 4d). Due to the synergistic effect of graphene and carbon layers, the structural stability of the material is highly improved. Hao focused on $Co_9S_8$ nanosheet arrays grown on carbon cloth under optimal nickel incorporation conditions. The addition of Ni can optimize the electronic structure of $Co_9S_8$ and improve the conductivity and charge transfer efficiency. In addition, the nanosheet structure endows a two-dimensional charge transfer pathway, exposing more active sites [50]. Tang and Fu both obtained N and S co-doped $Co_9S_8$ nanoplates [51,52]. Tang prepared nitrogen-sulfur double-doped graphene and quasihexagonal $Co_9S_8$ nanoplates by a simple ion assembly method (Figure 4e). Fu used $Co_9S_8$ nanosheets and ethyl orthosilicate to directly form two-dimensional carbon precursors and disperse them into thiourea solution, and then removed them through pyrolysis and template to obtain N and S co-doped $Co_9S_8$/NSC porous carbon plates.

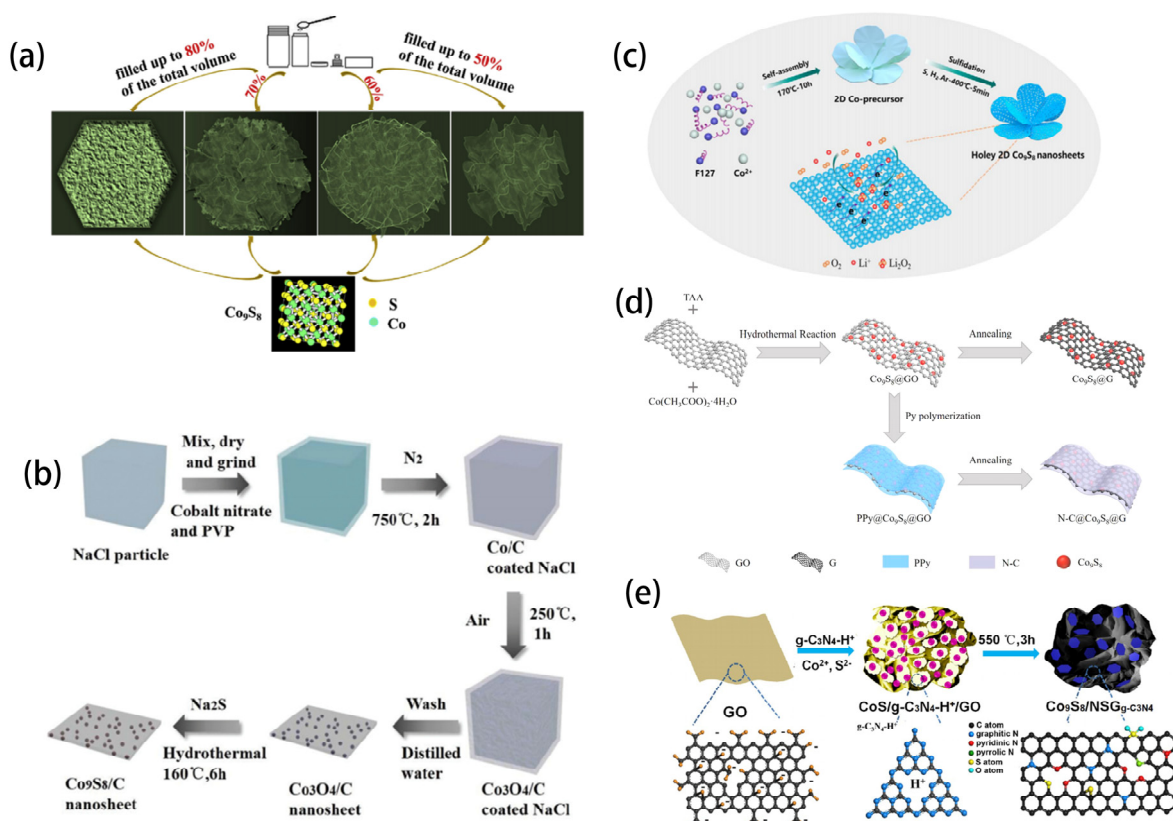**Figure 4.** (**a**) Schematic illustration of the controllable synthesis of $Co_9S_8$ catalysts. Reprinted with permission from Reference [42]. Copyright (2018) Elsevier Ltd. All rights reserved. (**b**) Schematic illustration of synthesis of $Co_9S_8/C$. Reprinted with permission from Reference [43]. Copyright (2019) Royal Society of Chemistry. (**c**) Schematic illustration for the synthesis of the holey $Co_9S_8$ nanosheets Reprinted with permission from Reference [46]. Copyright (2020) Elsevier Ltd. All rights reserved. (**d**) Schematic illustration of synthesis of N–C@$Co_9S_8$@G sandwich structure. Reprinted with permission from Reference [49]. Copyright (2020) Elsevier Ltd. All rights reserved. (**e**) Schematic demonstration of the preparation process for $Co_9S_8/NSG_{g-C3N4}$. Reprinted with permission from Reference [51]. Copyright (2017) American Chemical Society.

### 3.4. Three-Dimensional (3D) Structure

It is well known that the properties of nanomaterials depend on their morphology and size. Therefore, compared with 2D materials, 3D materials have a very wide application potential due to their controllable structure, large specific surface area, strong absorption capacity, superior electron and ion transport performance and additional advantages. Rajith Illathvalappil synthesized $Co_9S_8$-$Ni_3S_2$ layered nanoflower arrays which were self-supporting on nickel foam with the required porosity and structural characteristics using a one-pan hydrothermal method without using any adhesives (Figure 5a). The active modulation achieved in this experiment is attributed to the existence of the open pore morphology of $Co_9S_8$-$Ni_3S_2$ nanoflowers formed on the nickel foam, which is conducive to the adsorption of reactants and the transformation of gaseous products [53]. Xia successfully prepared a $Co_9S_8$-based photocatalyst for efficient hydrogen evolution (Figure 5b). They combined CdS quantum dots with hollow dodecahedron $Co_9S_8$ to form a $Co_9S_8/CdS$ heterostructure using a low-energy atmospheric single-pot strategy [54]. Similarly, Qiu designed a hollow cobalt sulfide cube embedded with cadmium sulfide quantum dots as a template using the one-pot hydrothermal method (Figure 5c). Hollow $CdS/Co_9S_8$ utilizes multi-light reflection in the cube structure to achieve enhanced photocatalytic activity [55]. Zhao synthesized $CoNi_2S_4/Co_9S_8$ nanostructures with high porosity, suitable pore size distribution and novel structure using simple chemical bath deposition [56].

By using a simple triethanolamine-assisted self-template strategy, Wang and colleagues prepared a unique three-dimensional honeycomb cobalt sulfide network composed of cross-linked nanosheets (Figure 5d). It was found for the first time that the introduction of triethanolamine in the reaction can effectively increase the proportion of high-priced $Co^{3+}$ in the final product [57]. Li reported the atomic layer deposition of cobalt sulfide. In this process, high quality $Co_9S_8$ films with layer-by-layer growth behavior were produced using $H_2S$ as reactant. $Co_9S_8$ films can also be conformally deposited into deep and narrow grooves with an aspect ratio of 10:1, which indicates that this process has a high application prospect for $Co_9S_8$ conformal coating on 3D nanostructures with elevated aspect ratio [58].
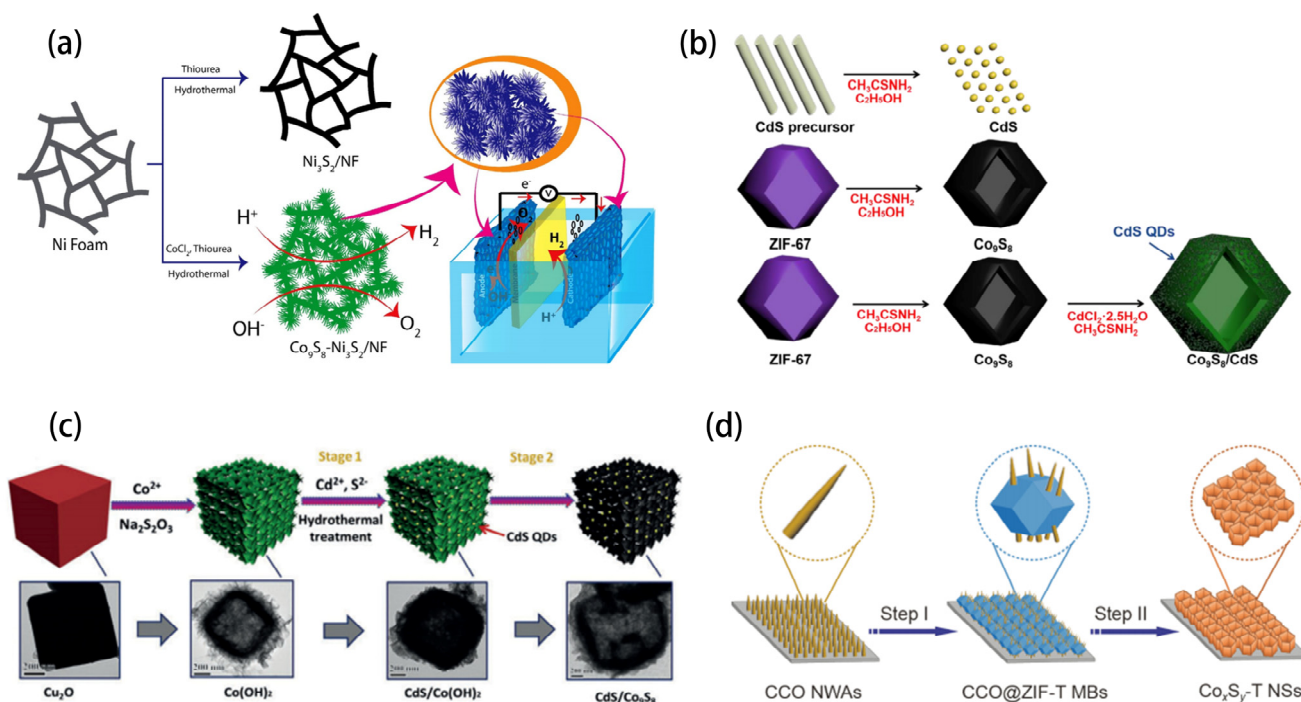


**Figure 5.** (**a**) Schematic illustration of the synthesis of $Co_9S_8$ -$Ni_3S_2$ /NF through the hydrothermal route and the use of this system as the bi-functional electrode in water electrolysis. Reprinted with permission from Reference [53]. Copyright (2020) Wiley-VCH. (**b**) Preparative Process for CdS, $Co_9S_8$, and $Co_9S_8$/CdS. Reprinted with permission from Reference [54]. Copyright (2021) American Chemical Society. (**c**) The preparative process for CdS/$Co_9S_8$ and corresponding TEM images; scale bar (200 nm). Reprinted with permission from Reference [55]. Copyright (2017) Wiley-VCH. (**d**) Schematic illustration of the formation of the $Co_xS_y$-TNSs. Reprinted with permission from Reference [57]. Copyright (2021) Springer Ltd. All rights reserved.

## 4. Applications

As mentioned above, $Co_9S_8$-based nanomaterials are technically valuable functional materials for various applications. For photocatalytic technology, the keys to its excellent light capture and charge transfer are its higher specific surface area, more abundant active sites, shorter charge carrier migration distance and electronic structure. In addition to being the matrix material, $Co_9S_8$-based nanomaterials also promote the transformation of reaction kinetics and finally improve the electrode output. In the following sections, we will selectively review some typical examples involving $Co_9S_8$-based nanomaterials.

### 4.1. Photoelectric Catalysis

4.1.1. Photocatalytic Hydrogen Evolution Reaction (HER)

$H_2$, as a high energy density zero-pollution emission energy carrier, is considered as a promising alternative to fossil fuels. In general, Pt-based materials have been shown to be the most effective HER catalysts. However, their high cost and low reserves make them

difficult to realize for large-scale industrial applications. Therefore, the development of greatly active and stable earth-rich catalysts to reduce or eliminate the dependence on noble metal-based catalysts for HER remains a great challenge. $Co_9S_8$-based catalysts have been used as $H_2$-generating catalysts for non-noble metals and great progress has been made. To further improve the catalytic performance of $Co_9S_8$-based catalysts, several modification strategies such as defect engineering, doping and heterojunction engineering have been developed. For example, Zhang fabricated $Co_9S_8$-based ultrathin sheets with a thickness of 4 to 6 nm that are rich in edge defects, cavity defects and dislocation defects. Moreover, the catalytic activity of hydrogen evolution was optimized by tuning the coordination solvent and pyrolysis parameters to control the defects of $Co_9S_8$-based nanosheets. As shown in Figure 6a,b, the apparent defects on the surface of $Co_9S_8$-based nanosheets were confirmed by HRTEM images. They also assessed the thickness of $Co_9S_8$-based nanosheets as ~4 nm by AFM analysis (Figure 6c) [47]. In addition to the defects mentioned above, appropriate heteroatomic doping can adjust the electronic structure, which is an effective way to improve the performance of the electrocatalyst for hydrogen evolution. N, S, P heteroatom-doped composites have attracted much attention due to their high HER activity [58–60]. Among them, the study found that phosphorous-doped metal sulfide is particularly interesting, because P atoms have a similar atomic radius and electronegativity to S atoms, which makes it easy for P atoms to be doped into sulfide by replacing S atoms to bond with metal atoms and cause lattice distortion [61,62]. Such small changes to the parent lattice structure may provide new active sites, optimize the adsorption energy of hydrogen, or regulate the electronic band structure, which may be beneficial to improve its electrocatalytic performance [63]. Gao's team systematically studied the effect of the amount of P doping on the electrocatalytic properties of $CoS_2$. Through theoretical and experimental studies, Jin and colleagues established ternary pyrite cobalt phosphorus sulfide (CoPS) as a HER electrocatalyst with high performance [64]. Although the above two have made great contributions to exploring the application of P-doped $CoS_2$ and CoPS to HER, there are few studies on the catalysis of P-doped $Co_{1-x}S$, $Co_9S_8$ and other cobalt sulfide compounds. Qu reported a general synthesis method for various P-doped cobalt sulfide compounds, including $CoS_2/Co_{1-x}S$, $Co_{1-x}S$ and $Co_9S_8$ phase [65] (Figure 6h,i). It is found that hydrothermal temperature has a crucial influence on the phase of final products. Therefore, different phase products are synthesized by controlling the hydrothermal temperature. Because P atoms and S atoms have a similar atomic radius and electronegativity, P atoms are easily doped into sulfide by replacing the S atoms and bonding with metal atoms, which leads to lattice distortion. Through experimental study and theoretical calculation, it is shown that the introduction of P can effectively improve the conductivity of cobalt sulfide and optimize the hydrogen adsorption energy. This study provides guidance for the design of P-doped $Co_9S_8$ and other cobalt sulfide compounds as HER electrocatalysts. In order to improve HER efficiency, the construction of heterogeneous catalysts is also a popular strategy at present. Wu successfully prepared $MoS_2/Co_9S_8$ heterostructure and showed excellent catalytic performance and good stability [66]. As shown in Figure 6f,g, $MoS_2$ is evenly distributed on the surface of $Co_9S_8$, which is conducive to $MoS_2$ exposing more boundary active sites. In addition, the heterostructure formed between $MoS_2$ and $Co_9S_8$ is more favorable for electron transfer. The LSV curve and Tafel slope results show that, as shown in Figure 6h,i, the heterogeneous structure of $MoS_2/Co_9S_8$ greatly improves HER catalytic performance. In summary, to obtain high performance $Co_9S_8$-based HER electrocatalysts, the following points should be paid more attention. The intrinsic activity of each active site was improved by optimizing the hydrogen adsorption energy of the electrocatalyst. Moreover, improving the conductivity of electrocatalysts is equally important for accelerating the charge transfer. Furthermore, attention should be paid to improving the macroscopic structure, hydrophilic and hydrophobic characteristics, and enhancing the mass diffusion between the $H_2$ catalyst and the electrolyte.

Photocatalysis as a green and efficient $H_2$-generation pathway has also received extensive attention [67–69]. $Co_9S_8$ is an interesting visible light active photocatalyst with a

special electronic structure, tunable optical properties and wide corresponding range of light. Despite the encouraging progress, the catalytic efficiency of pure $Co_9S_8$ photocatalysts is still not ideal. Therefore, coupling $Co_9S_8$ to a semiconductor with an appropriate bandgap to form a heterostructure is a successful technique to efficiently collect electrons and induce charge transfer at the interface. Taraka Prabhu Yendrapati constructed an efficient and stable $Co_9S_8@CdIn_2S_4$ heterostructure for the photocatalytic generation of $H_2$ in visible light [70]. On the basis of retaining the polyhedral form of $Co_9S_8$, $CdIn_2S_4$ is uniformly decorated on the $Co_9S_8$ cage, as shown in Figure 6j,l. Two photoactive sulfide semiconductors are reasonably incorporated, and this hollow heterostructure can effectively achieve the separation and transfer of photoinduced charge, providing a broad surface area and abundant exposure sites for the photocatalytic redox reaction, so that it has stronger light-trapping ability and significant HER catalytic activity.
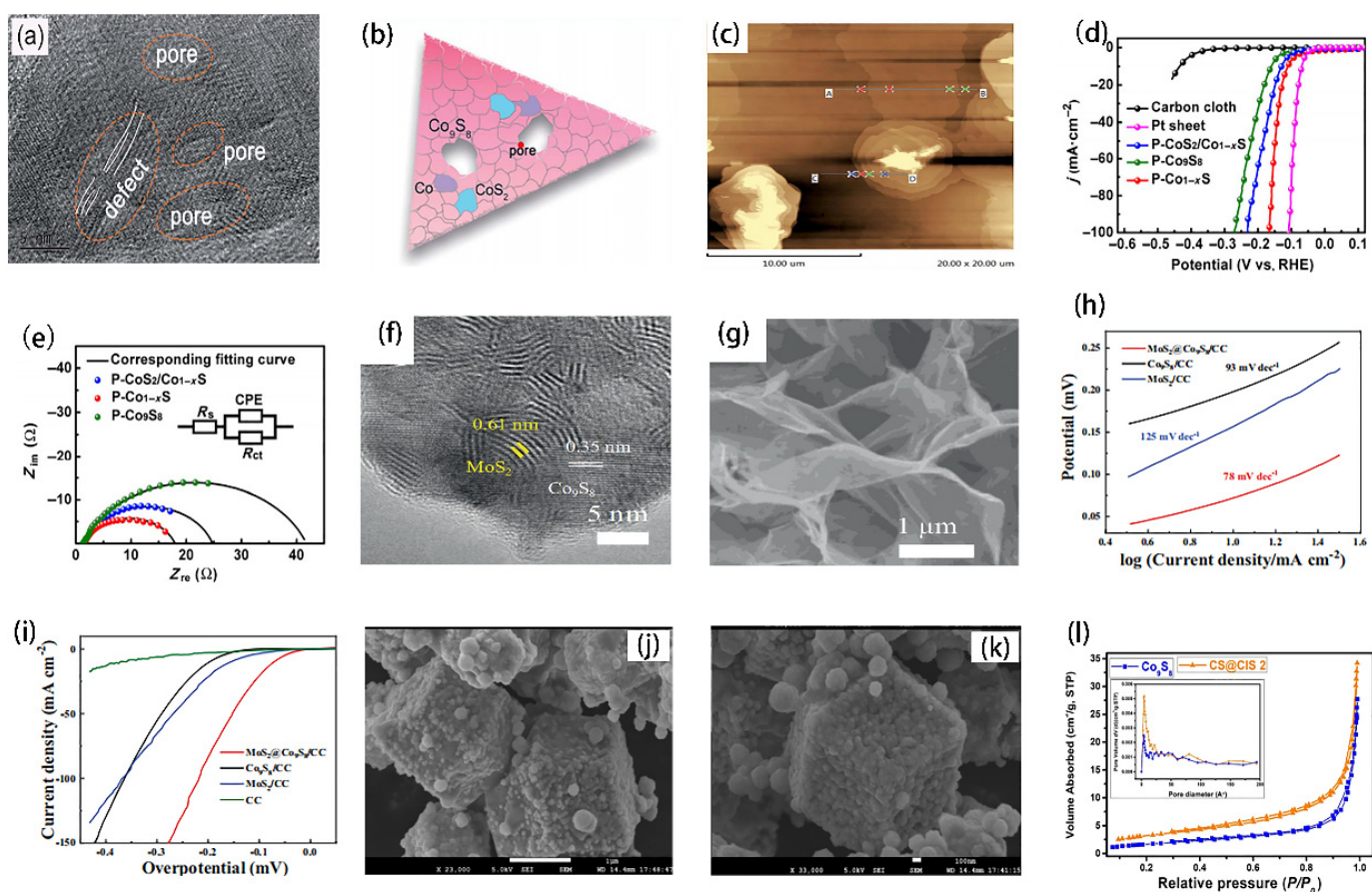


**Figure 6.** (**a**) HRTEM images of DR-$Co_9S_8$-II with pore defects and dislocation. (**b**) Schematic drawing of defective structures in DR-$Co_9S_8$-II nanosheets. (**c**) AFM images of DR-$Co_9S_8$-II. Reprinted with permission from Reference [47]. Copyright (2018) Royal Society of Chemistry. (**d**) LSV curves of bare carbon cloth, P-$Co_9S_8$, P-$Co_{1-x}S$, P-$CoS_2/Co_{1-x}S$ and Pt sheet. (**e**) Nyquist plots of P-$Co_9S_8$, P-$Co_{1-x}S$ and P-$CoS_2/Co_{1-x}S$. Reprinted with permission from Reference [65]. Copyright (2021) Elsevier Ltd. All rights reserved. (**f**) SEM images of $MoS_2@Co_9S_8/CC$. (**g**) HRTEM. The electrochemical measurements of all synthesized catalysts in 1 M KOH. (**h**) HER polarization curves. (**i**) Tafel plots. Reprinted with permission from Reference [66]. Copyright (2019) Springer Ltd. All rights reserved. (**j-l**) FESEM images of CS@CIS2 photocatalysts. Reprinted with permission from Reference [70]. Copyright (2021) American Chemical Society.

## 4.1.2. Electrocatalytic Water Splitting

With the exhaustion of non-renewable resources such as fossil fuels and the increasingly serious environmental pollution, people are focusing on renewable clean energy.

Electrochemical water decomposition is an efficient method to produce $H_2$ and $O_2$. Electrocatalytic water separation in the reaction process consists of two half reactions: HER at the cathode and OER at the anode. There are problems of high overpotential and slow kinetics in the reaction process. As a result, many scholars try to develop noble metal-free OER/HER dual-function catalysts to improve gas production rate and reduce energy consumption, among which, $Co_9S_8$-based materials have made great progress (Table 1). For example, Dong successfully prepared 1D $Co_9S_8$-$V_3S_4$/CC heterojunction dual-function electrocatalysis for water splitting and obtained good HER and OER performance, as shown in Figure 7a,b [34]. In this study, the researchers not only tested the performance of the catalyst, but also explained its catalytic mechanism. As shown in Figure 7c, XPS results confirmed the formation of the $Co_9S_8$-$V_3S_4$ heterojunction. It is noteworthy that the Co peak of $Co_9S_8$-$V_3S_4$/CC shifted to a positive position compared with $Co_9S_8$/CC and the V peak of $Co_9S_8$-$V_3S_4$/CC shifts negatively with respect to $V_3S_4$/CC. These results indicate that there is a strong electron interaction at the interface, where $V_3S_4$ acts as an electron attractor to obtain electrons from $Co_9S_8$, resulting in the higher $Co^{3+}$ and lower valence $V^{2+}$ states in $Co_9S_8$-$V_3S_4$/CC. In conclusion, the electron transfer from $Co_9S_8$ to $V_3S_4$ occurs at the interface due to the strong electron coupling effect of the $Co_9S_8$-$V_3S_4$ heterojunction, where the electron attraction of $V_3S_4$ ($V^{2+}$) optimizes the adsorption of H* active substance and is favorable for HER. The electron loss of $Co_9S_8$ ($Co^{3+}$) responds to the enhancement of OER activity. In addition to being a dual-function electrocatalyst, $Co_9S_8$-based materials are also widely used as three-function electrocatalysts. Based on the concept of sustainable energy development, Liang designed a three-function electrocatalytic material containing $Co_9S_8$/Co in situ encapsulated in N-doped carbon nanotubes (Figure 7d), achieving efficient electrocatalytic reactions of oxygen reduction, oxygen evolution and hydrogen evolution [71]. The microstructure analysis shows that $Co_9S_8$ and Co nanoparticles are in situ integrated into N-doped graphite carbon tube (Figure 7e). In this study, they highlight the importance of the rich Co-N and Co-N-C coupling centers generated by in situ engineering of the conversion of metal sulfides to carbon–nitrogen frameworks for the multifunctional catalytic conversion of sustainable energy. As shown in Figure 7f,g, XPS confirmed the existence of abundant Co-N and Co-N-C coupled active sites at the interface. In addition, Li also reported $Co_9S_8$ as a multifunctional electrocatalytic material [31]. The theoretical calculation and experimental results showed that the synergistic effect between $Co_9S_8$ nanoparticles and single cobalt atom will reduce the reaction barrier, as shown in Figure 7h,i, thus promoting the generation of ORR, OER and HER. According to the above studies, it can be concluded that bifunctional or even trifunctional catalysts with excellent HER and OER performance reflect the diversity of their catalytic functions and may show great potential in other types of applications [41].

**Table 1.** Electrocatalytic Activity of $Co_9S_8$-Based materials.

| Material | Electrolytes | OER (mV) | Tafel Slope (mV dec$^{-1}$) | HER (mV) | Tafel Slope (mV dec$^{-1}$) | Ref. |
|---|---|---|---|---|---|---|
| $Co_9S_8$-$V_3S_4$/CC | 1.0 M KOH | 232@10 mA cm$^{-2}$ | 59 | 85@10 mA cm$^{-2}$ | 51 | [34] |
| CdS@$Co_9S_8$/$Ni_3S_2$ | 1.0 M KOH | 285@20 mA cm$^{-2}$ | 96.8 | 69.6@-10 mA cm$^{-2}$ | 121 | [72] |
| $Co_9S_8$@$MoS_2$ | 1.0 M KOH | 342@10 mA cm$^{-2}$ | 94 | 147@10 mA cm$^{-2}$ | 117 | [73] |
| $MoO_2$@$MoS_2$@$Co_9S_8$ | 1.0 M KOH | 310@10 mA cm$^{-2}$ | 70 | 160@10 mA cm$^{-2}$ | 96 | [74] |
| $Co_9S_8$@$Ni(OH)_2$ | 1.0 M KOH | 140@60 mA cm$^{-2}$ | 70 | 119@10 mA cm$^{-2}$ | 80 | [41] |
| Mo-$Co_9S_8$/NF | 1.0 M KOH | 210@50 mA cm$^{-2}$ | - | 139@10 mA cm$^{-2}$ | - | [40] |
| $Co_9S_8$-$Ni_3S_2$ HNTs/Ni | 1.0 M KOH | 281@50 mA cm$^{-2}$ | 53.3 | 85@10 mA cm$^{-2}$ | 83.1 | [37] |
| $Co_9S_8$-$Ni_3S_2$ /NF | 1.0 M KOH | 102@25 mA cm$^{-2}$ | 105.3 | 227@25 mA cm$^{-2}$ | 171.2 | [53] |
| $Co_9S_8$/CNFs | 1.0 M KOH | 230@10 mA cm$^{-2}$ | 72 | 165@10 mA cm$^{-2}$ | 83 | [75] |
| Co/$Co_9S_8$-$MoS_2$ | 1.0 M KOH | 325@10 mA cm$^{-2}$ | 69 | 128@10 mA cm$^{-2}$ | 65 | [76] |
| $Co_9S_8$-NSC@$Mo_2C$ | 1.0 M KOH | 293@10 mA cm$^{-2}$ | 59.7 | 89@10 mA cm$^{-2}$ | 86.7 | [23] |
| $Co_9S_8$@NiCo LDH/NF | 1.0 M KOH | 278@30 mA cm$^{-2}$ | 83 | 168@10 mA cm$^{-2}$ | 103 | [77] |
| $Co_9S_8$/$Cu_2S$/CF | 1.0 M KOH | 195@10 mA cm$^{-2}$ | 78.8 | 165@10 mA cm$^{-2}$ | 80.2 | [78] |
| CFP@$Co_9S_8$@C | 1.0 M KOH | 290@10 mA cm$^{-2}$ | 74 | 175@10 mA cm$^{-2}$ | 97 | [33] |
| $Co_9S_8$/$Co_3O_4$ | 1.0 M KOH | 250@10 mA cm$^{-2}$ | 73.54 | - | - | [79] |
| Co/$Co_9S_8$@SNGS | 1.0 M KOH | 290@10 mA cm$^{-2}$ | 80.2 | 350@20 mA cm$^{-2}$ | 96.1 | [80] |
| $Co_9S_8$@$MoS_2$/N | 1.0 M KOH | 223@10 mA cm$^{-2}$ | 56.3 | 126@-10 mA cm$^{-2}$ | 74.1 | [81] |
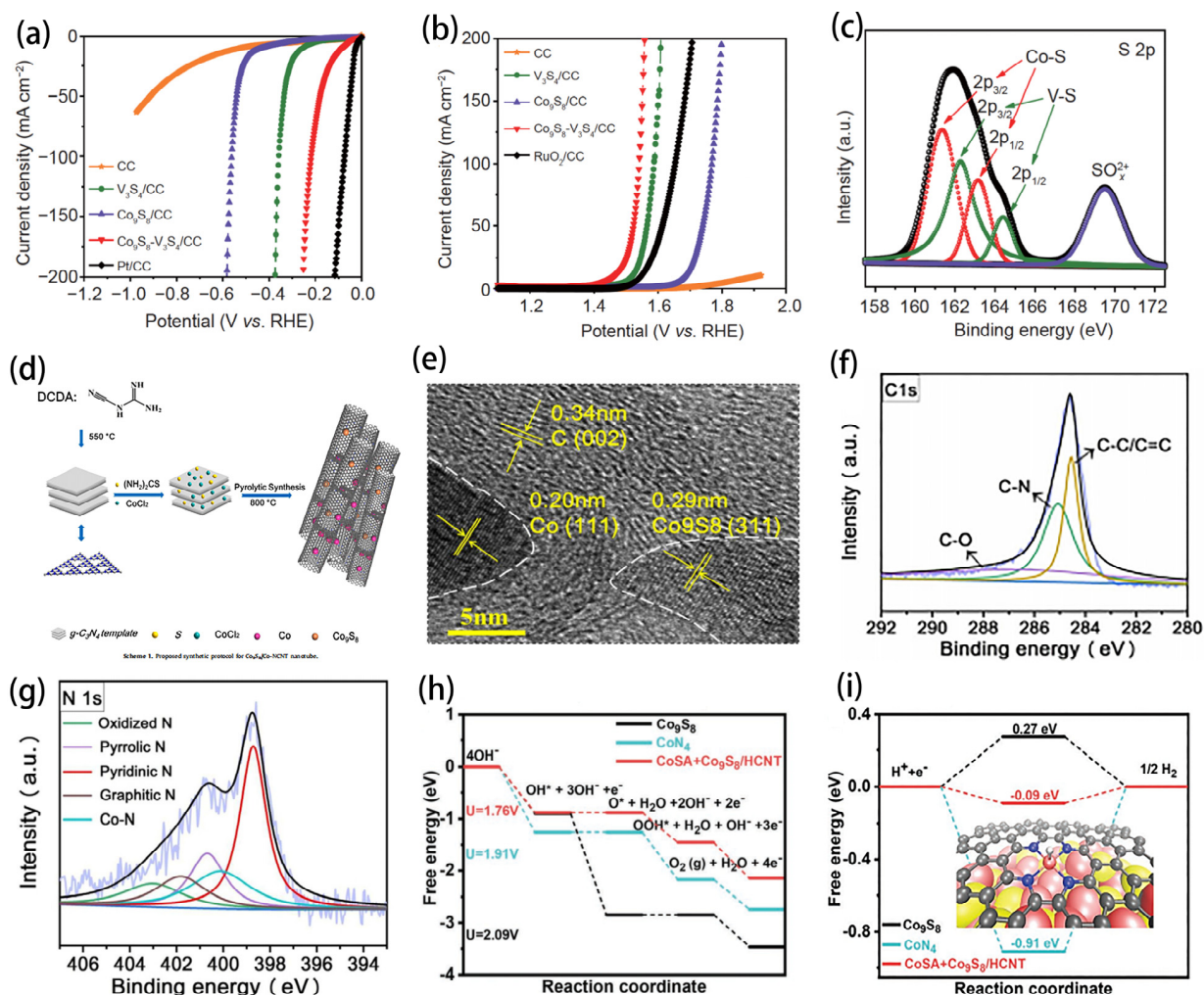


**Figure 7.** (**a**) Polarization curves of bare CC, $V_3S_4$/CC, $Co_9S_8$/CC, $Co_9S_8$-$V_3S_4$/CC and Pt-C/CC catalysts with a scan rate of 2 mV s$^{-1}$ in 1.0 mol L$^{-1}$ KOH for HER. (**b**) Polarization curves of bare CC,

$V_3S_4/CC$, $Co_9S_8/CC$, $Co_9S_8$-$V_3S_4/CC$ and $RuO_2/CC$ catalysts with a scan rate of 2 mV s$^{-1}$ in 1.0 mol L$^{-1}$ KOH for OER. (**c**) XPS survey spectrum of S 2p of $Co_9S_8$-$V_3S_4/CC$. Reprinted with permission from Reference [34]. Copyright (2019) Elsevier Ltd. All rights reserved. (**d**) Proposed synthetic protocol for $Co_9S_8$/Co-NCNT nanotube. (**e**) HRTEM images of $Co_9S_8$/Co-NCNT-0.05. (**f–g**) High resolution XPS spectra of $Co_9S_8$/Co-NCNT-0.05. Reprinted with permission from Reference [71]. Copyright (2020) Wiley-VCH. (**h**) Free energy diagrams for the thermodynamic limiting potentials of OER steps. (**i**) Free energy diagrams of $Co_9S_8$, $CoN_4$, and CoSA + $Co_9S_8$/HCNT for HER and inset is the model of adsorption configuration of HER on CoSA + $Co_9S_8$/HCNT. Reprinted with permission from Reference [31]. Copyright (2021) Springer Ltd. All rights reserved.

*4.2. Electrochemical Energy Storage*

Electrochemical energy storage devices such as supercapacitors, Li/Na ion batteries, Li-S batteries and Zn-air batteries play an important role in modern society. In order to follow the needs of social development, it is very desirable to obtain a better, new generation of batteries. Therefore, as a key component of energy storage devices, the performance of electrode materials is particularly important. $Co_9S_8$-based materials have the natural advantage of building better electrode materials. By carefully adjusting the chemical composition and microstructure of transition metal sulfides, significant electrical conductivity can be obtained, thus solving many existing problems and bringing significant development to supercapacitors and batteries.

4.2.1. Batteries

Lithium-Ion Batteries

Rechargeable lithium-ion batteries (LIBs) have been widely used in many modern electronic products, such as electric vehicles and portable electronic devices, due to their high energy density, environmental friendliness and long-term cycle stability. However, the theoretical capacity of graphite used as an anode material limits the development of LIBs. Transition metal $Co_9S_8$, which has become a high-performance LIBs electrode material, has been widely studied because of its large theoretical capacity and high safety. For example, as shown in Figure 8a, Chen prepared N and S co-doped carbon skeleton cobalt sulfide nanoparticles ($Co_9S_8$/NSC) by a one-step method [82]. As an anode for lithium-ion batteries, the composite material has good reversible capacity, high velocity performance and long-term cycling stability (Figure 8b,c). Although $Co_9S_8$-based nanomaterials have made great progress as electrode materials, their further development is still greatly hindered by their volume expansion and electrical conductivity. Therefore, many scholars adjust the structure of materials or compound $Co_9S_8$ with other materials to get better electrode materials [49,83,84]. He demonstrated an expandable electrostatic spinning method for preparing $Co_9S_8$/$Ni_3S_2$@S-CNFs materials as independent anode materials [85]. In particular, this study forms an independent 3D nanofiber network that allows lithium ions to easily access the active nanoparticles, thereby enhancing the activity and stability of the material.

Sodium-Ion Batteries

In recent years, with the increasing demand for low-cost, long-life, high-energy density storage systems, sodium ion batteries (SIBs) have been considered as a promising alternative to LIBs due to the abundant supply and low cost of sodium [86–88]. At present, $Co_9S_8$-based materials has good conductivity as SIBs electrode material and can be a cathode material with great potential for commercialization. Li and his colleagues demonstrated that the rich grain boundaries and three-layer exposed interfaces of the prepared $Co_9S_8$-carbon material are the main capacitors for the storage performance of high sodium ions through experiments and simulation analysis [89]. Wang and colleagues prepared $Co_9S_8$@S-CF materials by in situ pore-forming, sulfurization, sulfur doping, and carbonization [90]. As shown in Figure 8d, sulfur-doped foam carbon has abundant voids. These interstitial

spaces can construct three-dimensional ion/electron paths to accelerate the transport of sodium ions/electrons to $Co_9S_8$ nanoclusters. In addition, the reversible capacity retention rate is up to 80% after 1000 cycles, and the Coulomb efficiency is over 95%, which is very close to the theoretical capacity of hybrid material, as shown in Figure 8e. The results show that the material has a unique foam-like structure and is superior to $Co_9S_8$ nanosheets in terms of reversible capacity, capacity retention and cyclic stability. According to the above research, it can be found that $Co_9S_8$-based materials pave a new way for the development of advanced electrodes for SIBs, and can, therefore, be extended to the development of various metal sulfide based electrodes for SIBs.

Lithium–Sulfur Batteries

Lithium–sulfur batteries have been widely explored because of their rich sulfur resources and high energy density, which overcomes the limitations of existing energy storage devices [91–93]. However, there are still many limitations that restrict the large-scale commercial development of lithium–sulfur batteries, such as large volume changes, irreversible loss of soluble lithium polysulfide in electrolytes and reduced number of electrochemical active reaction sites. To address the above technical obstacles, $Co_9S_8$-based nanomaterials can be combined with the electrode matrix to maximize the use of sulfur and inhibit the dissolution of polysulfides due to their excellent physical and chemical properties. Chen proposed that injecting $Co_9S_8$ into N-doped graphene to improve the electronic conductivity of the base. It is worth noting that the highly polar $Co_9S_8$ is considered to be an excellent chemical adsorbent and catalyst. It not only effectively immobilized the soluble lithium polysulfide through chemical binding, but also significantly catalyzed the electrochemical conversion of the soluble lithium polysulfide, and finally, inhibited its shuttle effect [94]. In addition, Li prepared $Co_9S_8$-doped graphene as the main material for a lithium–sulfur battery [95]. As shown in Figure 8f, the electron spin resonance spectrum verified the presence of sulfur vacancies in the sample. The use of UV-Vis adsorption spectrum indicates that the sulfur vacancy generated in the material effectively improves the adsorption capacity of polysulfide anions. In addition, density functional theory has calculated the adsorption energy of the material for polysulfide (Figure 8g,h). Finally, electrochemical experiments showed that the sulfur vacancy promoted the electrode kinetics of polysulfide catalytic conversion. The results showed that it is an effective way to develop high performance lithium–sulfur batteries by using sulfur vacancy to enhance sulfur conversion kinetics. Although the $Co_9S_8$-based materials play a role in promoting the performance of Li-S batteries, the shuttle effect, large amount of variation of sulfur and the formation of polysulfide have not been completely solved, and the real reality of Li-S batteries still needs a lot of exploration.
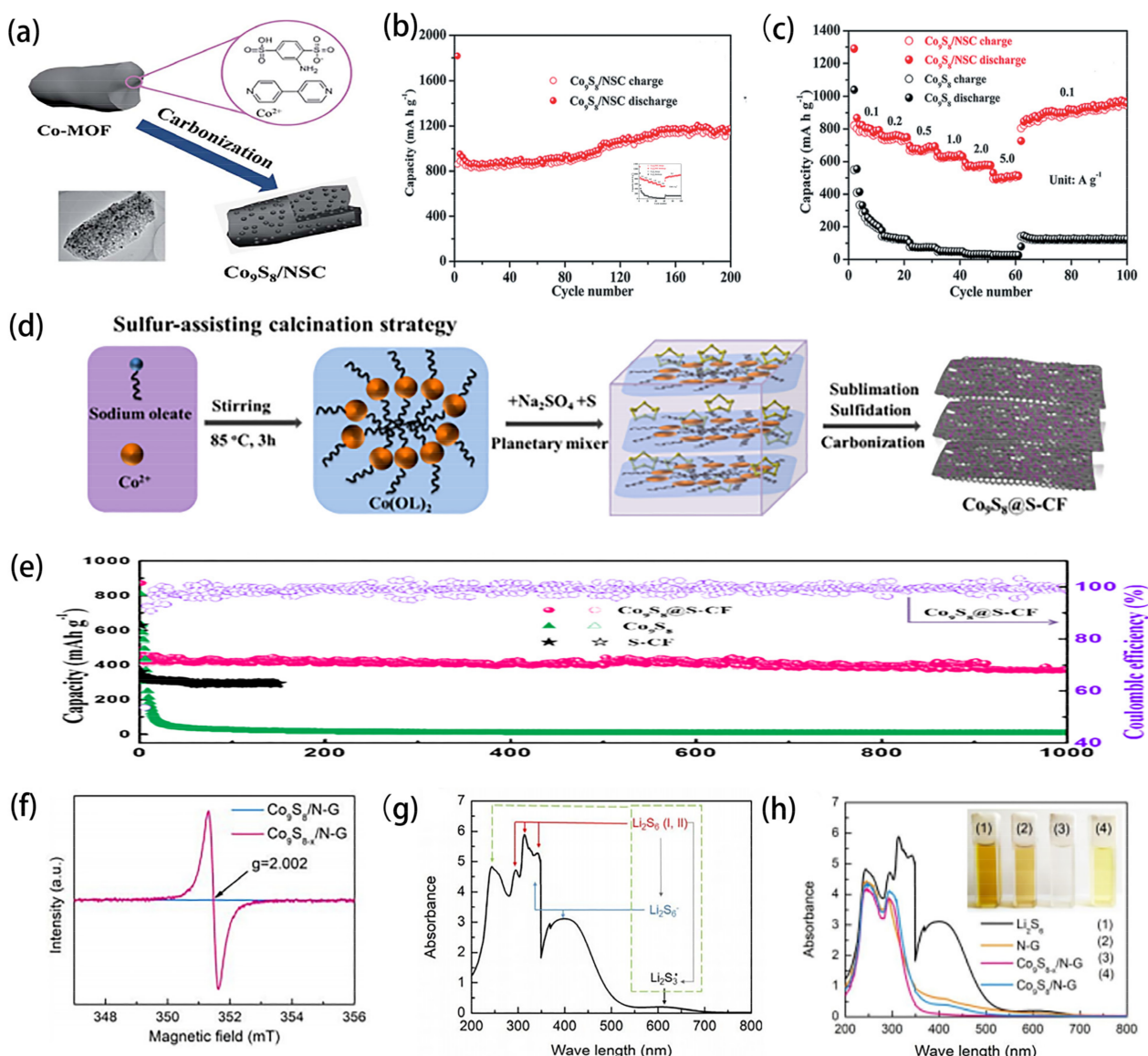
**Figure 8.** (**a**) Schematic drawing of the formation process to obtain the hybrid composite $Co_9S_8$/NSC. (**b**) the cycling performance at 0.1 A g 1 of $Co_9S_8$/NSC. (**c**) rate capability. Reprinted with permission from Reference [82]. Copyright (2019) Royal Society of Chemistry. (**d**) Schematic illustration for in situ formation of $Co_9S_8$ nanoclusters confined in sulfur-doped carbon foam (denoted as $Co_9S_8$@S-CF). (**e**) Cycling performance of the $Co_9S_8$@S-CF and $Co_9S_8$ nanosheets and S-CF electrodes at 0.25 C (1 C = 400 mA g$^{-1}$). Reprinted with permission from Reference [90]. Copyright (2019) American Chemical Society. (**f**) Electron spin resonance spectra of $Co_9S_8$/N-doped graphene and $Co_9S_8$-x/N-doped graphene. (**g**) Assignment of absorption bands in UV-Vis spectrum of $Li_2S_6$ DOL/DME solution. (**h**) UV-Vis spectra of the $Li_2S_6$ solution and after static adsorption of the different host materials. Reprinted with permission from Reference [95]. Copyright (2013) Royal Society of Chemistry.

### Zn-Air Batteries

Dual-function electrocatalytic materials are an important part of many renewable energy devices. For example, in the water splitting mentioned above, HER and OER are the two main reactions. In metal–air batteries, the ORR and OER activity at the side of the air electrode is a key parameter that determines the performance of the battery, and the voltage difference between the two reactions determines the efficiency and energy consumption of the device. Although a simple mixture of a single catalytically active catalyst can also

achieve the effect of dual-function catalyst, the corresponding energy density and power density will decrease owing to the increase of mass load. Therefore, it is reasonable to study the corresponding dual-function catalysts, especially for demanding batteries. $Co_9S_8$-based materials are an excellent choice for metal–air batteries, especially for zinc–air batteries, due to their excellent bi-functional properties in ORR and OER [96,97]. Zheng synthesized a series of N- and S-doped carbon $NSC/Co_9S_8$ materials. Considering that the structure of the electrode material is an important factor in the optimization of the electrocatalyst, they introduced homogeneous mesopores or macropores in the carbon structure [98]. Excellent electrocatalytic activity of the oxygen reduction reaction was obtained, which was mainly due to the improvement of wettability and the interaction with $O_2$. Although $Co_9S_8$ is a promising non-noble metal bi-functional electrocatalyst, the electrocatalytic performance of cobalt-based nanocatalysts is still unsatisfactory due to the poor electrical conductivity and easy aggregation during continuous operation. In order to solve the above problems, Cao synthesized the honeycomb structure porous carbon ($Co_9S_8$/NSC) in situ composite by a simple method inspired by honeycomb in nature [99]. $Co_9S_8$ nanoparticles embedded in the carbon matrix of a 3D interconnection network gave it high electrical conductivity, which not only promoted the electron transfer and charge transfer at the interface, but also promoted the exposure and rapid transfer of active sites of ORR/OER-related species, and the obtained composite material exhibited high cyclic stability.

### 4.2.2. Supercapacitors

Supercapacitors have become a research hotspot because of their advantages, such as high power density, high coulomb efficiency and long cycle span [100,101]. In the field of energy storage, supercapacitors play an important role in complementing or even replacing conventional batteries. However, capacitors still have disadvantages beyond battery devices, such as low energy density and self-discharge. Therefore, in order to improve the electrochemical performance of supercapacitors, many scholars have conducted a lot of research and gained some new understandings. For example, only specific functional groups such as pyridine- or pyrrole-type nitrogen are favorable for Faraday reactions, the transfer of electrons and ions on the surface is critical to the rate capacity, and the morphology is also related to electrochemical properties [102–104]. In addition, it is also crucial to find excellent electrode materials for capacitors. $Co_9S_8$-based materials can improve the conductivity by introducing a pseudocapacitance reaction, expanding specific surface area and constructing porous structure [105,106].

Based on the above, $Co_9S_8$-based materials provide a good opportunity to construct capacitor electrodes with excellent performance. In order to further improve the conductivity of $Co_9S_8$-based materials in supercapacitor electrodes, Emad S. Goda successfully designed a novel structure encapsulated by nitrogen-doped graphene (Al-doped $Co_9S_8$@NG) as the positive electrode of the capacitor [107]. As shown in Figure 9a,b, the composite developed has a maximum capacity value of about 736 C/g at a current density of 1 A/g and has an ultra-long cycle stability after 10,000 cycles. These results indicate that carbon substrate, as a fast charge transfer agent, can balance the change of electrode volume and enhance the conductivity of nanoparticles, thus obtaining electrodes with good electrochemical characteristics. However, in addition to electrical conductivity, the structural instability of $Co_9S_8$-based materials often reduces their electrocatalytic activity during the long-term cycle, and reasonable improvement of their structural stability is still a challenge for energy conversion and storage applications. Wang used density functional theory to predict the stability of $Co_9S_8$, as shown in Figure 9c–f [108]. The calculation results show that compared with pure $Co_9S_8$, Fe that is doped in an octahedral position can improve its stability. In order to verify the theoretical results, $Co_9S_8$ hollow spheres with different Co/Fe molar ratios were prepared by one-step hydrothermal experiment and showed excellent electrocatalytic performance. As shown in Figure 9g–i, the Tafel slope is 63.9 mV $dec^{-1}$ and its overpotential is 268 mV at the current density of 10 mA $cm^{-2}$. To be sure, these impressive

findings open the door to the use of $Co_9S_8$-based materials as electrodes for high-efficiency energy storage capacitors.
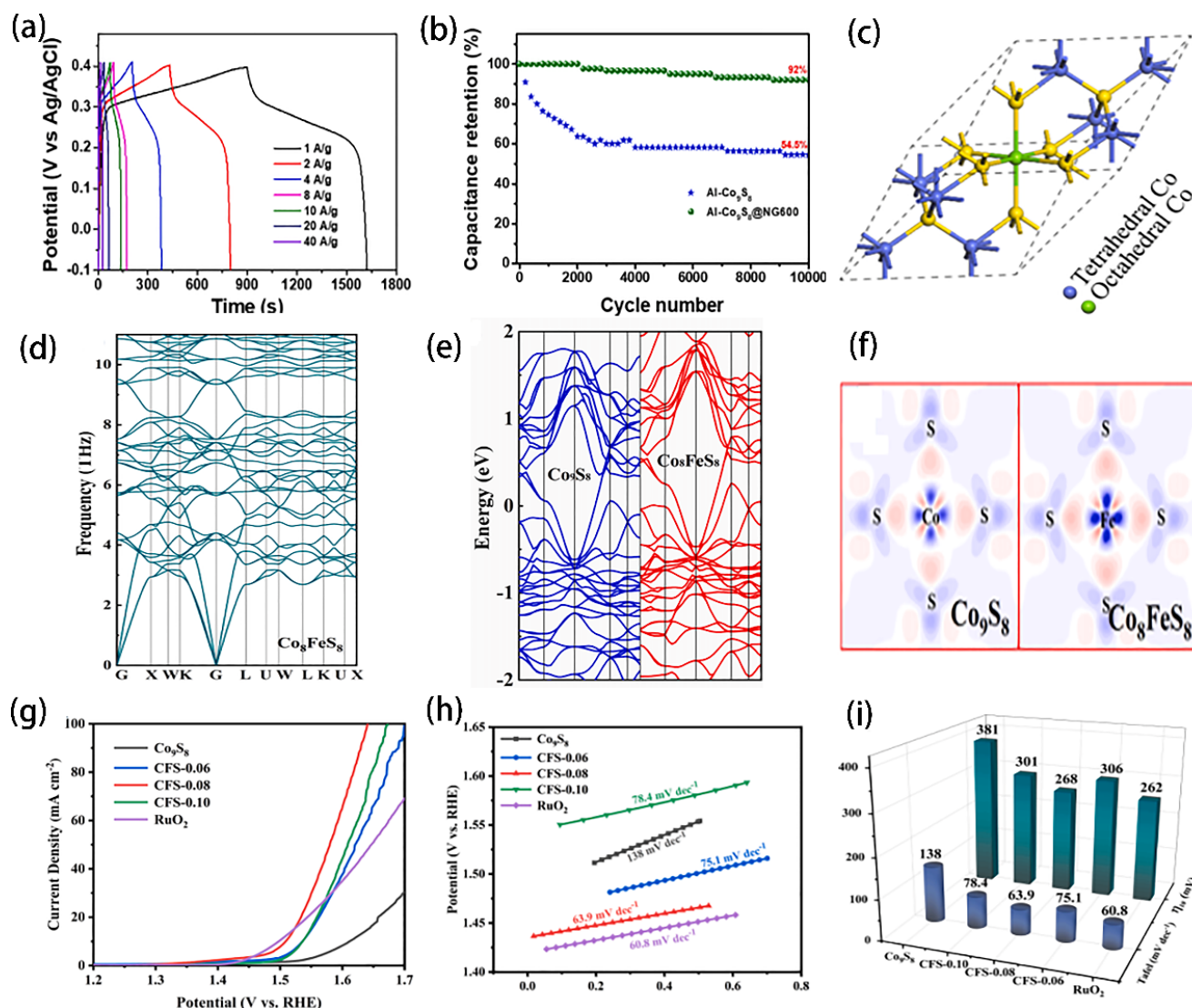


**Figure 9.** (**a**) GCD patterns performed at various applied current densities from 1 to 40 A/g for core-shell Al-$Co_9S_8$@NG600. (**b**) Cyclic life analysis for Al-$Co_9S_8$, Al- $Co_9S_8$@NG600 electrodes at an applied current density value of 20 A/g. Reprinted with permission from Reference [107]. Copyright (2022) Elsevier Ltd. All rights reserved. (**c**) The primitive unit cell of $Co_9S_8$, Green is octahedral metal, Blue is tetrahedral metal, and Yellow is sulfurs. (**d**) The phonon dispersions of $Co_8FeS_8$. (**e**) Calculated band structures. (**f**) charge density difference. (For interpretation of the references to colour in this figure legend, the reader is referred to the web version of this article). (**g**) The LSV curves for different catalysts in 1.0 M KOH at 5 mV s$^{-1}$. (**h**) Tafel slopes. (**i**) Corresponding overpotential at 10 mA cm$^{-2}$ and Tafel slopes of different catalysts, respectively. Reprinted with permission from Reference [108]. Copyright (2022) Elsevier Ltd. All rights reserved.

## 5. Conclusions and Outlooks

This paper reviews the theoretical and experimental results of non-noble metal $Co_9S_8$-based materials in photoelectric catalysis and electrochemical energy storage. These results provide valuable reference for further elucidating the reaction mechanism of catalyst or electrode materials. In addition, the physicochemical properties and synthesis strategies of $Co_9S_8$-based materials with different dimensions are discussed in detail. It should be noted

that there are still some key issues that need to be resolved and explored, even though the excellent properties of $Co_9S_8$-based materials facilitate their application in many fields.

(i)   The research regarding their reaction mechanism was not thorough, which restricts the further development of $Co_9S_8$-based materials as excellent catalyst and electrode materials.

(ii)  As an ideal catalyst, excellent results in different pH must be shown to make the water splitting process more efficient. However, experimental studies have shown that the proton concentration is bound to change during the HER process, which leads to different degrees of influence on $Co_9S_8$-based materials working in acidic or alkaline media.

(iii) Some renewable energy installations typically require excellent bi-functional catalytic performance, such as the Zn-air batteries mentioned above. However, the role of bi-functional catalytic activity in different electrolytes is not the same, which hinders its practical application.

(iv)  We review the applications of $Co_9S_8$-based materials as photocatalysts and energy storage materials in recent years, but not limited to this, we can also explore its applications in biosensors, organic catalytic synthesis and other new fields, which are of great value for facilitating multi-field applications.

In summary, $Co_9S_8$-based materials have shown great advantages as catalysts and electrode materials, but their applications in other fields remain a challenge. Therefore, this paper mainly aims to introduce the research progress of properties, preparation strategies and applications of $Co_9S_8$-based materials in different dimensions. It provides reference for better design of $Co_9S_8$-based materials for wider applications to alleviate these challenges. We believe that the extraordinary physical and chemical properties of $Co_9S_8$-based materials will enable exciting advances in high performance energy storage devices and energy applications in the future.

**Author Contributions:** Conceptualization and writing, C.W. and X.P.; investigation and supervision, G.W. and L.G.; validation, F.F. All authors have read and agreed to the published version of the manuscript.

**Institutional Review Board Statement:** Not applicable.

**Informed Consent Statement:** Not applicable.

**Data Availability Statement:** Not applicable.

**Conflicts of Interest:** The authors declare no conflict of interest.

## References

1. Long, J.; Gong, Y.; Lin, J. Metal-organic framework-derived $Co_9S_8@CoS@CoO@C$ nanoparticles as efficient electro-and photo-catalysts for the oxygen evolution reaction. *J. Mater. Chem. A* **2017**, *5*, 10495–10509. [CrossRef]
2. Riaz, M.S.; Yuan, X.; Zhao, Y.; Dong, C.; Nong, S.; Ali, Z.; Huang, F. Porous $NiCo_2S_4/Co_9S_8$ microcubes templated by sacrificial ZnO spheres as an efficient bifunctional oxygen electrocatalyst. *Adv. Sustain. Syst.* **2019**, *3*, 1800167. [CrossRef]
3. Chen, T.-T.; Wang, R.; Li, L.-K.; Li, Z.-J.; Zang, S.-Q. MOF-derived $Co_9S_8/MoS_2$ embedded in tri-doped carbon hybrids for efficient electrocatalytic hydrogen evolution. *J. Energy Chem.* **2020**, *44*, 90–96. [CrossRef]
4. Li, X.; Lv, X.; Sun, X.; Yang, C.; Zheng, Y.-Z.; Yang, L.; Li, S.; Tao, X. Edge-oriented, high-percentage 1T′-phase $MoS_2$ nanosheets stabilize $Ti_3C_2$ MXene for efficient electrocatalytic hydrogen evolution. *Appl. Catal. B Environ.* **2021**, *284*, 119708. [CrossRef]
5. Hu, C.; Ma, K.; Hu, Y.; Chen, A.; Saha, P.; Jiang, H.; Li, C. Confining $MoS_2$ nanocrystals in MOF-derived carbon for high performance lithium and potassium storage. *Green Energy Environ.* **2021**, *6*, 75–82. [CrossRef]
6. Ma, G.; Xu, X.; Feng, Z.; Hu, C.; Zhu, Y.; Yang, X.; Yang, J.; Qian, Y. Carbon-coated mesoporous $Co_9S_8$ nanoparticles on reduced graphene oxide as a long-life and high-rate anode material for potassium-ion batteries. *Nano Res.* **2020**, *13*, 802–809. [CrossRef]
7. Xing, Y.; Li, D.; Li, L.; Tong, H.; Jiang, D.; Shi, W. Accelerating water dissociation kinetic in $Co_9S_8$ electrocatalyst by mn/N Co-doping toward efficient alkaline hydrogen evolution. *Int. J. Hydrogen Energy* **2021**, *46*, 7989–8001. [CrossRef]

8. Liu, H.; Ma, X.; Hu, H.; Pan, Y.; Zhao, W.; Liu, J.; Zhao, X.; Wang, J.; Yang, Z.; Zhao, Q. Robust NiCoP/CoP heterostructures for highly efficient hydrogen evolution electrocatalysis in alkaline solution. *ACS Appl. Mater. Inter.* **2019**, *11*, 15528–15536. [CrossRef]

9. Zhu, H.; Zhang, J.; Yanzhang, R.; Du, M.; Wang, Q.; Gao, G.; Wu, J.; Wu, G.; Zhang, M.; Liu, B. When cubic cobalt sulfide meets layered molybdenum disulfide: A core–shell system toward synergetic electrocatalytic water splitting. *Adv. Mater.* **2015**, *27*, 4752–4759. [CrossRef]

10. Heidelberg, R.F.; Luxem, A.H.; Talhouk, S.; Banewicz, J.J. The magnetic susceptibilities of the cobalt-sulfur system. *Inorg. Chem.* **1966**, *5*, 194–197. [CrossRef]

11. Dutková, E.; Čaplovičová, M.; Škorvánek, I.; Baláž, M.; Zorkovská, A.; Baláž, P.; Čaplovič, Ľ. Structural, surface and magnetic properties of chalcogenide $Co_9S_8$ nanoparticles prepared by mechanochemical synthesis. *Inorg. Chem.* **2018**, *745*, 863–867. [CrossRef]

12. Zhou, Y.X.; Yao, H.B.; Wang, Y.; Liu, H.L.; Gao, M.R.; Shen, P.K.; Yu, S.H. Hierarchical hollow $Co_9S_8$ microspheres: Solvothermal synthesis, magnetic, electrochemical, and electrocatalytic properties. *Chem. Eur. J.* **2010**, *16*, 12000–12007. [CrossRef]

13. Lai, C.-H.; Lu, M.-Y.; Chen, L.-J. Metal sulfide nanostructures: Synthesis, properties and applications in energy conversion and storage. *J. Mater. Chem.* **2012**, *22*, 19–30. [CrossRef]

14. Li, H.; Qian, X.; Xu, C.; Huang, S.; Zhu, C.; Jiang, X.; Shao, L.; Hou, L. Hierarchical porous $Co_9S_8$/nitrogen-doped carbon@$MoS_2$ polyhedrons as pH universal electrocatalysts for highly efficient hydrogen evolution reaction. *ACS Appl. Mater. Inter.* **2017**, *9*, 28394–28405. [CrossRef]

15. Dong, D.; Wu, Z.; Wang, J.; Fu, G.; Tang, Y. Recent progress in $Co_9S_8$ -based materials for hydrogen and oxygen electrocatalysis. *J. Mater. Chem. A* **2019**, *7*, 16068–16088. [CrossRef]

16. Kalimuldina, G.; Nurpeissova, A.; Adylkhanova, A.; Adair, D.; Taniguchi, I.; Bakenov, Z. Morphology and dimension variations of copper sulfide for high-performance electrode in rechargeable batteries: A review. *ACS Appl. Enegr. Mater.* **2020**, *3*, 11480–11499. [CrossRef]

17. Pokropivny, V.; Skorokhod, V. Classification of nanostructures by dimensionality and concept of surface forms engineering in nanomaterial science. *Mater. Sci. Eng. C* **2007**, *27*, 990–993. [CrossRef]

18. Feng, L.-L.; Li, G.-D.; Liu, Y.; Wu, Y.; Chen, H.; Wang, Y.; Zou, Y.-C.; Wang, D.; Zou, X. Carbon-armored $Co_9S_8$ nanoparticles as all-pH efficient and durable $H_2$-evolving electrocatalysts. *ACS Appl. Mater. Inter.* **2015**, *7*, 980–988. [CrossRef]

19. Wang, M.; Zhou, J.; Cheng, S.; Pan, Q.; Yao, M.; Zhu, Y.; Wu, P.; Luo, H.; Yang, L.; Liu, M. Template synthesis of carbon-coated $Co_9S_8$ composite with largely improved capacity for lithium ion batteries. *Mater. Res. Lett.* **2018**, *217*, 163–166. [CrossRef]

20. Liu, X.; Li, Q.; Zhao, Y.; Dong, Y.; Fan, Q.; Kuang, Q. A promising mechanical ball-milling method to synthesize carbon-coated $Co_9S_8$ nanoparticles as high-performance electrode for supercapacitor. *J. Mater. Sci.* **2017**, *52*, 13552–13560. [CrossRef]

21. Lu, M.; Liao, C.; Jiang, C.; Du, Y.; Zhang, Z.; Wu, S. Remarkable high-temperature performance of hollow $Co_9S_8$ nanoparticles integrated with carbon materials for lithium-ion batteries. *Electrochim. Acta* **2017**, *250*, 196–202. [CrossRef]

22. Zhang, S.; Li, D.; Chen, S.; Yang, X.; Zhao, X.; Zhao, Q.; Komarneni, S.; Yang, D. Highly stable supercapacitors with MOF-derived $Co_9S_8$/carbon electrodes for high rate electrochemical energy storage. *J. Mater. Chem. A* **2017**, *5*, 12453–12461. [CrossRef]

23. Luo, X.; Zhou, Q.; Du, S.; Li, J.; Zhong, J.; Deng, X.; Liu, Y. Porous $Co_9S_8$/nitrogen, sulfur-doped carbon@ $Mo_2C$ dual catalyst for efficient water splitting. *ACS Appl. Mater. Inter.* **2018**, *10*, 22291–22302. [CrossRef] [PubMed]

24. Du, J.; Wang, R.; Lv, Y.-R.; Wei, Y.-L.; Zang, S.-Q. One-step MOF-derived Co/$Co_9S_8$ nanoparticles embedded in nitrogen, sulfur and oxygen ternary-doped porous carbon: An efficient electrocatalyst for overall water splitting. *Chem. Commun.* **2019**, *55*, 3203–3206. [CrossRef] [PubMed]

25. Wang, S.; Zhou, G.; Lv, J.; Ma, Y.; Wang, Y.; Hu, C.; Zhang, J.; Yang, J.; He, G.; Zhang, M. $Co_9S_8$/CoS@S, N co-doped porous carbon derived from MOFs as an efficient catalyst for the oxygen evolution reaction. *J. Phys. Chem. Solids* **2021**, *148*, 109696. [CrossRef]

26. Yu, H.; Sun, X.; Tang, D.; Huang, Y.; Zhang, W.; Miao, S.; Qiao, Z.-A.; Wang, J.; Zhao, Z. Molten salt strategy to synthesize alkali metal-doped $Co_9S_8$ nanoparticles embedded, N, S co-doped mesoporous carbon as hydrogen evolution electrocatalyst. *Int. J. Hydrogen Energy* **2020**, *45*, 6006–6014. [CrossRef]

27. Yu, H.; Tang, D.; Huang, Y.; Zhang, W.; Sun, X.; Yang, X.; Qiao, Z.A.; Wang, J.; Zhao, Z. Nitrogen and Sulfur Co-Doped Mesoporous Carbon Embedded with $Co_9S_8$ Nanoparticles: Efficient Electrocatalysts for Hydrogen Evolution. *Chempluschem* **2019**, *84*, 1604–1609. [CrossRef]

28. Yu, H.; Zhang, W.; Miao, S.; Du, Y.; Huang, Y.; Tang, D.; Qiao, Z.-A.; Wang, J.; Zhao, Z. Synthesis of $Co_9S_8$ nanoparticle embedded, N, S Co-doped mesoporous carbon with salts as templates for electrocatalytic hydrogen evolution. *Micropor. Mesopor. Mat* **2020**, *302*, 110235. [CrossRef]

29. Zhang, P.; Bin, D.; Wei, J.-S.; Niu, X.-Q.; Chen, X.-B.; Xia, Y.-Y.; Xiong, H.-M. Efficient oxygen electrocatalyst for Zn–air batteries: Carbon dots and $Co_9S_8$ nanoparticles in a N, S-codoped carbon matrix. *ACS Appl. Mater. Inter.* **2019**, *11*, 14085–14094. [CrossRef]

30. Wang, S.; Wang, X.; Xie, Y.; Jiang, W.; Wang, X.; Jiang, Y.; Zhou, W.; Pan, K. In situ growth of $Co_9S_8$ nanocrystals on reduced graphene oxide for the enhanced catalytic performance of dye-sensitized solar cell. *J. Alloys Compd.* **2019**, *803*, 216–223. [CrossRef]

31. Li, Y.; Cao, R.; Li, L.; Tang, X.; Chu, T.; Huang, B.; Yuan, K.; Chen, Y. Simultaneously integrating single atomic cobalt sites and $Co_9S_8$ nanoparticles into hollow carbon nanotubes as trifunctional electrocatalysts for Zn–air batteries to drive water splitting. *Small* **2020**, *16*, 1906735. [CrossRef]

32. Zhang, N.; Wang, W.; Teng, C.; Wu, Z.; Ye, Z.; Zhi, M.; Hong, Z. Co$_9$S$_8$ nanoparticle-decorated carbon nanofibers as high-performance supercapacitor electrodes. *RSC Adv.* **2018**, *8*, 27574–27579. [CrossRef]

33. Yang, Q.; Liu, L.; Xiao, L.; Zhang, L.; Wang, M.J.; Li, J.; Wei, Z. Co$_9$S$_8$@N, S-codoped carbon core–shell structured nanowires: Constructing a fluffy surface for high-density active sites. *J. Mater. Chem. A* **2018**, *6*, 14752–14760. [CrossRef]

34. Dong, X.; Jiao, Y.; Yang, G.; Yan, H.; Wu, A.; Guo, D.; Wang, Y.; Tian, C.; Fu, H. One-dimensional CO$_9$S$_8$-V$_3$S$_4$ heterojunctions as bifunctional electrocatalysts for highly efficient overall water splitting. *Sci. China Mater.* **2021**, *64*, 1396–1407. [CrossRef]

35. Liu, M.; Wang, L.; Yu, X.; Zhang, H.; Zhang, H.; Li, S.; Huang, F. Introducing oxygen vacancies for improving the electrochemical performance of Co$_9$S$_8$@NiCo-LDH nanotube arrays in flexible all-solid battery-capacitor hybrid supercapacitors. *Energy* **2022**, *238*, 121767. [CrossRef]

36. Zhu, F.; Yan, M.; Liu, Y.; Shen, H.; Lei, Y.; Shi, W. Hexagonal prism-like hierarchical Co$_9$S$_8$@Ni(OH)$_2$ core–shell nanotubes on carbon fibers for high-performance asymmetric supercapacitors. *J. Mater. Chem. A* **2017**, *5*, 22782–22789. [CrossRef]

37. Li, J.; Xu, P.; Zhou, R.; Li, R.; Qiu, L.; Yuan, D. Co$_9$S$_8$-Ni$_3$S$_2$ heterointerfaced nanotubes on Ni foam as highly efficient and flexible bifunctional electrodes for water splitting. *Electrochim. Acta* **2019**, *299*, 152–162. [CrossRef]

38. Zhang, G.; Chen, D.; Li, N.; Xu, Q.; Li, H.; He, J.; Lu, J. Construction of hierarchical hollow Co$_9$S$_8$/ZnIn$_2$S$_4$ tubular heterostructures for highly efficient solar energy conversion and environmental remediation. *Angew. Chem.* **2020**, *132*, 8332–8338. [CrossRef]

39. Wu, L.; Zhang, K.; Wang, T.; Xu, X.; Zhao, Y.; Sun, Y.; Zhong, W.; Du, Y. Cobalt Sulfide Nanotubes (Co$_9$S$_8$) Decorated with Amorphous MoSx as Highly Efficient Hydrogen Evolution Electrocatalyst. *ACS Appl. Nano Mater.* **2018**, *1*, 1083–1093. [CrossRef]

40. Du, X.; Ma, G.; Zhang, X. Mo-doped Co$_9$S$_8$ nanorod array as a high performance electrochemical water splitting catalyst in alkaline solution. *Int. J. Hydrogen Energy* **2019**, *44*, 27765–27771. [CrossRef]

41. Du, X.; Huang, C.; Zhang, X. Surface modification of a Co$_9$S$_8$ nanorods with Ni(OH)$_2$ on nickel foam for high water splitting performance. *Int. J. Hydrogen Energy* **2019**, *44*, 19953–19966. [CrossRef]

42. Yang, Y.; Yuan, M.; Li, H.; Sun, G.; Ma, S. Controllable synthesis of ultrathin Co$_9$S$_8$ nanosheets as a highly efficient electrocatalyst for overall water splitting. *Electrochim. Acta* **2018**, *281*, 198–207. [CrossRef]

43. Li, L.; Song, L.; Guo, H.; Xia, W.; Jiang, C.; Gao, B.; Wu, C.; Wang, T.; He, J. N-Doped porous carbon nanosheets decorated with graphitized carbon layer encapsulated Co$_9$S$_8$ nanoparticles: An efficient bifunctional electrocatalyst for the OER and ORR. *Nanoscale* **2019**, *11*, 901–907. [CrossRef] [PubMed]

44. Zhang, C.Y.; Lu, Z.W.; Wang, Y.H.; Dai, Z.; Zhao, H.; Sun, G.Z.; Lan, W.; Pan, X.J.; Zhou, J.Y.; Xie, E.Q. Cooperative chemisorption of polysulfides via 2D hexagonal WS$_2$-rimmed Co$_9$S$_8$ heterostructures for lithium–sulfur batteries. *Chem. Eng. J.* **2020**, *392*, 123734. [CrossRef]

45. Xing, L.; Dong, Y.; Wu, X. Hierarchical Co$_3$O$_4$@Co$_9$S$_8$ nanowall structures assembled by many nanosheets for high performance asymmetric supercapacitors. *RSC. Adv.* **2018**, *8*, 28172–28178. [CrossRef]

46. Wang, G.; Li, Y.; Shi, L.; Qian, R.; Wen, Z. Realizing the growth of nano-network Li$_2$O$_2$ film on defect-rich holey Co$_9$S$_8$ nanosheets for Li-O$_2$ battery. *Chem. Eng. J.* **2020**, *396*, 125228. [CrossRef]

47. Zhang, X.; Liu, Y.; Gao, J.; Han, G.; Hu, M.; Wu, X.; Cao, H.; Wang, X.; Li, B. Defect-rich (Co–CoS$_2$)$_x$@Co$_9$S$_8$ nanosheets derived from monomolecular precursor pyrolysis with excellent catalytic activity for hydrogen evolution reaction. *J. Mater. Chem. A* **2018**, *6*, 7977–7987. [CrossRef]

48. Wang, X.; Su, D.; Xiao, Y.; Xu, S.; Fang, S.; Cao, S. Ultra-dispersed island-like Co$_9$S$_8$ nanoparticles composed of nanosheets in-situ grown on nitrogen-doped graphene for asymmetric supercapacitor. *Electrochim. Acta* **2019**, *293*, 419–425. [CrossRef]

49. Li, N.; Sun, L.; Wang, K.; Xu, S.; Zhang, J.; Guo, X.; Liu, X. Sandwiched N-carbon@Co$_9$S$_8$@Graphene nanosheets as high capacity anode for both half and full lithium-ion batteries. *J. Energy Chem.* **2020**, *51*, 62–71. [CrossRef]

50. Hao, P.; Zhu, W.; Li, L.; Tian, J.; Xie, J.; Lei, F.; Cui, G.; Zhang, Y.; Tang, B. Nickel incorporated Co$_9$S$_8$ nanosheet arrays on carbon cloth boosting overall urea electrolysis. *Electrochim. Acta* **2020**, *338*, 135883. [CrossRef]

51. Tang, Y.; Jing, F.; Xu, Z.; Zhang, F.; Mai, Y.; Wu, D. Highly crumpled hybrids of nitrogen/sulfur dual-doped graphene and Co$_9$S$_8$ nanoplates as efficient bifunctional oxygen electrocatalysts. *ACS Appl. Mater. Inter.* **2017**, *9*, 12340–12347. [CrossRef]

52. Fu, S.; Zhu, C.; Song, J.; Feng, S.; Du, D.; Engelhard, M.H.; Xiao, D.; Li, D.; Lin, Y. Two-dimensional N, S-codoped carbon/Co$_9$S$_8$ catalysts derived from Co(OH)$_2$ nanosheets for oxygen reduction reaction. *ACS Appl. Mater. Inter.* **2017**, *9*, 36755–36761. [CrossRef]

53. Illathvalappil, R.; Walko, P.S.; Kanheerampockil, F.; Bhat, S.K.; Devi, R.N.; Kurungot, S. Hierarchical Nanoflower Arrays of Co$_9$S$_8$-Ni$_3$S$_2$ on Nickel Foam: A Highly Efficient Binder-Free Electrocatalyst for Overall Water Splitting. *Chem. Eur. J.* **2020**, *26*, 7900–7911. [CrossRef]

54. Xia, C.; Xue, C.; Bian, W.; Liu, J.; Wang, J.; Wei, Y.; Zhang, J. Hollow Co$_9$S$_8$/CdS nanocages as efficient photocatalysts for hydrogen evolution. *ACS Appl. Nano Mater.* **2021**, *4*, 2743–2751. [CrossRef]

55. Qiu, B.; Zhu, Q.; Du, M.; Fan, L.; Xing, M.; Zhang, J. Efficient solar light harvesting CdS/Co$_9$S$_8$ hollow cubes for Z-scheme photocatalytic water splitting. *Angew. Chem. Int. Ed.* **2017**, *56*, 2684–2688. [CrossRef]

56. Zhao, F.; Huang, W.; Zhang, H.; Zhou, D. Facile synthesis of CoNi$_2$S$_4$/Co$_9$S$_8$ composites as advanced electrode materials for supercapacitors. *Appl. Surf. Sci.* **2017**, *426*, 1206–1212. [CrossRef]

57. Wang, H.; Yang, Y.; Li, Q.; Lu, W.; Ning, J.; Zhong, Y.; Zhang, Z.; Hu, Y. Molecule-assisted modulation of the high-valence Co$^{3+}$ in 3D honeycomb-like CoxSy networks for high-performance solid-state asymmetric supercapacitors. *Sci. China Mater.* **2021**, *64*, 840–851. [CrossRef]

58. Li, Y.-W.; Wu, Q.; Ma, R.-C.; Sun, X.-Q.; Li, D.-D.; Du, H.-M.; Ma, H.-Y.; Li, D.-C.; Wang, S.-N.; Dou, J.-M. A Co-MOF-derived $Co_9S_8$@NS-C electrocatalyst for efficient hydrogen evolution reaction. *RSC Adv.* **2021**, *11*, 5947–5957. [CrossRef]

59. Li, M.; Zhou, H.; Yang, W.; Chen, L.; Huang, Z.; Zhang, N.; Fu, C.; Kuang, Y. $Co_9S_8$ nanoparticles embedded in a N, S co-doped graphene-unzipped carbon nanotube composite as a high performance electrocatalyst for the hydrogen evolution reaction. *J. Mater. Chem. A* **2017**, *5*, 1014–1021. [CrossRef]

60. Liu, R.; Zhang, H.; Zhang, X.; Wu, T.; Zhao, H.; Wang, G. $Co_9S_8$@N, P-doped porous carbon electrocatalyst using biomass-derived carbon nanodots as a precursor for overall water splitting in alkaline media. *RSC Adv.* **2017**, *7*, 19181–19188. [CrossRef]

61. Brumme, T.; Calandra, M.; Mauri, F. First-principles theory of field-effect doping in transition-metal dichalcogenides: Structural properties, electronic structure, Hall coefficient, and electrical conductivity. *Phys. Rev. B* **2015**, *91*, 155436. [CrossRef]

62. Liu, W.; Hu, E.; Jiang, H.; Xiang, Y.; Weng, Z.; Li, M.; Fan, Q.; Yu, X.; Altman, E.I.; Wang, H. A highly active and stable hydrogen evolution catalyst based on pyrite-structured cobalt phosphosulfide. *Nat. Commun.* **2016**, *7*, 1–9. [CrossRef] [PubMed]

63. Zhang, J.; Liu, Y.; Xia, B.; Sun, C.; Liu, Y.; Liu, P.; Gao, D. Facile one-step synthesis of phosphorus-doped $CoS_2$ as efficient electrocatalyst for hydrogen evolution reaction. *Electrochim. Acta* **2018**, *259*, 955–961. [CrossRef]

64. Cabán-Acevedo, M.; Stone, M.L.; Schmidt, J.; Thomas, J.G.; Ding, Q.; Chang, H.-C.; Tsai, M.-L.; He, J.-H.; Jin, S. Efficient hydrogen evolution catalysis using ternary pyrite-type cobalt phosphosulphide. *Nat. Matem.* **2015**, *14*, 1245–1251. [CrossRef] [PubMed]

65. Qu, G.; Wu, T.; Yu, Y.; Wang, Z.; Zhou, Y.; Tang, Z.; Yue, Q. Rational design of phosphorus-doped cobalt sulfides electrocatalysts for hydrogen evolution. *Nano Res.* **2019**, *12*, 2960–2965. [CrossRef]

66. Wu, J.; Wang, X.; Jiang, J.; Lin, W.; Zhu, S.; Sha, J.; Ma, L.; Zhao, N. In-situ synthesis of $MoS_2$/$Co_9S_8$ heterostructure for efficient HER electrocatalyst. *Mater. Lett.* **2021**, *292*, 129621. [CrossRef]

67. Su, P.; Liu, H.; Ma, Q.; Jin, Z. $Mn_{0.05}Cd_{0.95}S$ decorated MOF-derived $Co_9S_8$ hollow polyhedron for efficient photocatalytic hydrogen evolution. *Int. J. Energy Res.* **2021**, *45*, 13040–13054. [CrossRef]

68. Li, X.-l.; He, R.-b.; Dai, Y.-j.; Li, S.-s.; Xiao, N.; Wang, A.-x.; Gao, Y.-q.; Li, N.; Gao, J.-f.; Zhang, L.-h. Design and fabrication of $Co_9S_8$/$Zn_{0.5}Cd_{0.5}S$ hollow nanocages with significantly enhanced photocatalytic hydrogen production activity. *Chem. Eng. J.* **2020**, *400*, 125474. [CrossRef]

69. Li, C.; Zhao, Y.; Liu, X.; Huo, P.; Yan, Y.; Wang, L.; Liao, G.; Liu, C. Interface engineering of $Co_9S_8$/$CdIn_2S_4$ ohmic junction for efficient photocatalytic $H_2$ evolution under visible light. *J. Colloid Interf. Sci.* **2021**, *600*, 794–803. [CrossRef]

70. Yendrapati, T.P.; Soumya, J.; Bojja, S.; Pal, U. Robust $Co_9S_8$@$CdIn_2S_4$ cage for efficient photocatalytic $H_2$ evolution. *J. Phys. Chem. C* **2021**, *125*, 5099–5109. [CrossRef]

71. Liang, D.; Mao, J.; Liu, P.; Yan, J.; Song, W. In-situ growth of NCNT and encapsulation of $Co_9S_8$/Co as a sustainable multifunctional electrocatalyst. *J. Colloid Interf. Sci.* **2019**, *557*, 291–300. [CrossRef]

72. Si, F.; Tang, C.; Gao, Q.; Peng, F.; Zhang, S.; Fang, Y.; Yang, S. Bifunctional CdS@$Co_9S_8$/$Ni_3S_2$ catalyst for efficient electrocatalytic and photo-assisted electrocatalytic overall water splitting. *J. Mater. Chem. A* **2020**, *8*, 3083–3096. [CrossRef]

73. Bai, J.; Meng, T.; Guo, D.; Wang, S.; Mao, B.; Cao, M. $Co_9S_8$@$MoS_2$ core-shell heterostructures as trifunctional electrocatalysts for overall water splitting and Zn-air batteries. *ACS Appl. Mater. Inter.* **2018**, *10*, 1678–1689. [CrossRef]

74. Li, Y.; Wang, C.; Cui, M.; Xiong, J.; Mi, L.; Chen, S. Heterostructured $MoO_2$@$MoS_2$@$Co_9S_8$ nanorods as high efficiency bifunctional electrocatalyst for overall water splitting. *Appl. Surf. Sci.* **2021**, *543*, 148804. [CrossRef]

75. Gu, L.; Zhu, H.; Yu, D.; Zhang, S.; Chen, J.; Wang, J.; Wan, M.; Zhang, M.; Du, M. A facile strategy to synthesize cobalt-based self-supported material for electrocatalytic water splitting. *Part. Part. Syst. Char.* **2017**, *34*, 1700189. [CrossRef]

76. Lin, Q.; Liang, J.; Liu, J.; Zhang, Q.; Peng, W.; Li, Y.; Zhang, F.; Fan, X. Hierarchical amorphous carbon-coated Co/$Co_9S_8$ nanoparticles on $MoS_2$ toward synergetic electrocatalytic water splitting. *Ind. Eng. Chem. Res.* **2019**, *58*, 23093–23098. [CrossRef]

77. Yan, J.; Chen, L.; Liang, X. $Co_9S_8$ nanowires@NiCo LDH nanosheets arrays on nickel foams towards efficient overall water splitting. *Sci. Bull.* **2019**, *64*, 158–165. [CrossRef]

78. Zang, Z.; Wang, X.; Li, X.; Zhao, Q.; Li, L.; Yang, X.; Yu, X.; Zhang, X.; Lu, Z. $Co_9S_8$ nanosheet coupled $Cu_2S$ nanorod heterostructure as efficient catalyst for overall water splitting. *ACS Appl. Mater. Inter.* **2021**, *13*, 9865–9874. [CrossRef]

79. Peng, D.; Zhang, B.; Wu, J.; Huang, K.; Cao, X.; Lu, Y.; Zhang, Y.; Li, C.; Huang, Y. Growth of Lattice Coherent $Co_9S_8$/$Co_3O_4$ Nano-Heterostructure for Maximizing the Catalysis of Co-Based Composites. *Chemcatchem* **2020**, *12*, 2431–2435. [CrossRef]

80. Zhang, X.; Liu, S.; Zang, Y.; Liu, R.; Liu, G.; Wang, G.; Zhang, Y.; Zhang, H.; Zhao, H. Co/$Co_9S_8$@S, N-doped porous graphene sheets derived from S, N dual organic ligands assembled Co-MOFs as superior electrocatalysts for full water splitting in alkaline media. *Nano Energy* **2016**, *30*, 93–102. [CrossRef]

81. Kim, M.; Seok, H.; Selvam, N.C.S.; Cho, J.; Choi, G.H.; Nam, M.G.; Kang, S.; Kim, T.; Yoo, P.J. Kirkendall effect induced bifunctional hybrid electrocatalyst ($Co_9S_8$@$MoS_2$/N-doped hollow carbon) for high performance overall water splitting. *J. Power Source* **2021**, *493*, 229688. [CrossRef]

82. Chen, L.; Yang, W.; Li, X.; Han, L.; Wei, M. $Co_9S_8$ embedded into N/S doped carbon composites: In situ derivation from a sulfonate-based metal-organic framework and its electrochemical properties. *J. Mater. Chem. A* **2019**, *7*, 10331–10337. [CrossRef]

83. Xiao, X.; Zhang, Z.; Yang, K.; Mei, T.; Yan, D.; Wang, X. Design and synthesize hollow spindle Ni-doped $Co_9S_8$@ZnS composites and their enhanced cycle performance. *J. Alloys Compd.* **2021**, *853*, 157118. [CrossRef]

84. Zhao, S.; Tian, X.; Zhou, Y.; Ma, B.; Natarajan, A. Three-dimensionally interconnected $Co_9S_8$/MWCNTs composite cathode host for lithium-sulfur batteries. *J. Energy Chem.* **2020**, *46*, 22–29. [CrossRef]

85. He, Z.; Guo, H.; LaCoste, J.D.; Cook, R.A.; Hussey, B.; Zhang, X.; Gang, D.D.; Hao, J.; Chen, L.; Cooke, P. Directly embedded $Ni_3S_2/Co_9S_8$@S-doped carbon nanofiber networks as a free-standing anode for lithium-ion batteries. *Sustain. Energy Fuels* **2021**, *5*, 166–174. [CrossRef]

86. Yin, M.; Zhao, D.; Feng, C.; Zhou, W.; Jiao, Q.; Feng, X.; Wang, S.; Zhao, Y.; Li, H.; Feng, T. Construction of porous $Co_9S_8$ hollow boxes with double open ends toward high-performance half/full sodium-ion batteries. *ACS Sustain. Chem. Eng.* **2020**, *8*, 6305–6314. [CrossRef]

87. Zhou, Y.; Zhang, J.; Sun, F.; Yu, X.; Kang, W.; Zhang, J. One-step synthesis of $Co_9S_8$@$Ni_3S_2$ heterostructure for enhanced electrochemical performance as sodium ion battery anode material and hydrogen evolution electrocatalyst. *J. Solid State Chem.* **2020**, *285*, 121230. [CrossRef]

88. Yin, M.; Feng, X.; Zhao, D.; Zhao, Y.; Li, H.; Zhou, W.; Liu, H.; Bai, X.; Wang, H.; Feng, C. Hierarchical $Co_9S_8$@carbon hollow microspheres as an anode for sodium ion batteries with ultralong cycling stability. *ACS Sustain. Chem. Eng.* **2019**, *7*, 6122–6130. [CrossRef]

89. Li, X.; Li, K.; Zhu, S.; Fan, K.; Lyu, L.; Yao, H.; Li, Y.; Hu, J.; Huang, H.; Mai, Y.W. Fiber-in-Tube Design of $Co_9S_8$-Carbon/$Co_9S_8$: Enabling Efficient Sodium Storage. *Angew. Chem.* **2019**, *131*, 6305–6309. [CrossRef]

90. Wang, Y.; Wang, Y.; Wang, Y.-x.; Feng, X.; Chen, W.; Qian, J.; Ai, X.; Yang, H.; Cao, Y. In situ formation of $Co_9S_8$ nanoclusters in sulfur-doped carbon foam as a sustainable and high-rate sodium-ion anode. *ACS Appl. Mater. Inter.* **2019**, *11*, 19218–19226. [CrossRef]

91. Liu, X.; Wang, D.; Yang, X.; Zhao, Z.; Yang, H.; Feng, M.; Zhang, W.; Zheng, W. Synergistic dual-confinement effect: Merit of hollowly metallic $Co_9S_8$ in packaging enhancement of electrochemical performance of Li-S batteries. *ACS Appl. Energy Mater.* **2019**, *2*, 1428–1435. [CrossRef]

92. Zhang, H.; Ma, J.; Huang, M.; Shang, H.; Jiang, J.; Qiao, Y.; Liu, W.; Zhou, H.; Li, T.; Zhou, X. MOF-derived $Co_9S_8$/C hollow polyhedra grown on 3D graphene aerogel as efficient polysulfide mediator for long-life Li-S batteries. *Mater. Lett.* **2020**, *277*, 128331. [CrossRef]

93. Chen, T.; Ma, L.; Cheng, B.; Chen, R.; Hu, Y.; Zhu, G.; Wang, Y.; Liang, J.; Tie, Z.; Liu, J. Metallic and polar $Co_9S_8$ inlaid carbon hollow nanopolyhedra as efficient polysulfide mediator for lithium-sulfur batteries. *Nano Energy* **2017**, *38*, 239–248. [CrossRef]

94. Chen, L.; Wang, J.; Ren, Y.; Zeng, W. N-doped graphene embellished with $Co_9S_8$ enable advanced sulfur cathode for high-performance lithium-sulfur batteries. *Int. J. Energy Res.* **2020**, *44*, 4961–4968. [CrossRef]

95. Li, H.-J.; Song, Y.-H.; Xi, K.; Wang, W.; Liu, S.; Li, G.-R.; Gao, X.-P. Sulfur vacancies in $Co_9S_{8-x}$/N-doped graphene enhancing the electrochemical kinetics for high-performance lithium–sulfur batteries. *J. Mater. Chem. A* **2021**, *9*, 10704–10713. [CrossRef]

96. Huang, L.; Zuo, L.; Yu, T.; Wang, H.; He, Z.; Zhou, H.; Su, S.; Bian, T. Two-dimensional Co/$Co_9S_8$ nanoparticles decorated N, S dual-doped carbon composite as an efficient electrocatalyst for zinc-air battery. *J. Alloys Compd.* **2022**, *897*, 163108. [CrossRef]

97. Peng, W.; Wang, Y.; Yang, X.; Mao, L.; Jin, J.; Yang, S.; Fu, K.; Li, G. $Co_9S_8$ nanoparticles embedded in multiple doped and electrospun hollow carbon nanofibers as bifunctional oxygen electrocatalysts for rechargeable zinc-air battery. *Appl. Catal. B Environ.* **2020**, *268*, 118437. [CrossRef]

98. Zheng, Q.; Xiong, Y.; Tang, K.; Wu, M.; Hu, H.; Zhou, T.; Wu, Y.; Cao, Z.; Sun, J.; Yu, X. Modulation of pore-size in N, S-codoped carbon/$Co_9S_8$ hybrid for a stronger $O_2$ affinity toward rechargable zinc-air battery. *Nano Energy* **2022**, *92*, 106750. [CrossRef]

99. Cao, Z.-Q.; Wu, M.-Z.; Hu, H.-B.; Liang, G.-J.; Zhi, C.-Y. Monodisperse $Co_9S_8$ nanoparticles in situ embedded within N, S-codoped honeycomb-structured porous carbon for bifunctional oxygen electrocatalyst in a rechargeable Zn–air battery. *NPG Asia Mater.* **2018**, *10*, 670–684. [CrossRef]

100. Wang, G.; Zhang, L.; Zhang, J. A review of electrode materials for electrochemical supercapacitors. *Chem. Soc. Rev.* **2012**, *41*, 797–828. [CrossRef]

101. Béguin, F.; Presser, V.; Balducci, A.; Frackowiak, E. Carbons and Electrolytes for Advanced Supercapacitors. *Adv. Mater.* **2014**, *26*, 2219–2251. [CrossRef] [PubMed]

102. Khattak, A.M.; Ghazi, Z.A.; Liang, B.; Khan, N.A.; Iqbal, A.; Li, L.; Tang, Z. A redox-active 2D covalent organic framework with pyridine moieties capable of faradaic energy storage. *J. Mater. Chem. A* **2016**, *4*, 16312–16317. [CrossRef]

103. Ito, Y.; Christodoulou, C.; Nardi, M.V.; Koch, N.; Kläui, M.; Sachdev, H.; Müllen, K. Tuning the magnetic properties of carbon by nitrogen doping of its graphene domains. *J. Am. Chem. Soc.* **2015**, *137*, 7678–7685. [CrossRef] [PubMed]

104. Yu, M.; Lin, D.; Feng, H.; Zeng, Y.; Tong, Y.; Lu, X. Boosting the energy density of carbon-based aqueous supercapacitors by optimizing the surface charge. *Angew. Chem.* **2017**, *129*, 5546–5551. [CrossRef]

105. Sun, S.; Luo, J.; Qian, Y.; Jin, Y.; Liu, Y.; Qiu, Y.; Li, X.; Fang, C.; Han, J.; Huang, Y. Metal–Organic Framework Derived Honeycomb $Co_9S_8$@C Composites for High-Performance Supercapacitors. *Adv. Energy Mater.* **2018**, *8*, 1801080. [CrossRef]

106. Liu, S.; Tong, M.; Liu, G.; Zhang, X.; Wang, Z.; Wang, G.; Cai, W.; Zhang, H.; Zhao, H. S, N-containing Co-MOF derived $Co_9S_8$@S, N-doped carbon materials as efficient oxygen electrocatalysts and supercapacitor electrode materials. *Inorg. Chem. Front.* **2017**, *4*, 491–498. [CrossRef]

107. Goda, E.S.; ur Rehman, A.; Pandit, B.; Eissa, A.A.-S.; Hong, S.E.; Yoon, K.R. Al-doped Co$_9$S$_8$ encapsulated by nitrogen-doped graphene for solid-state asymmetric supercapacitors. *Chem. Eng. J.* **2022**, *428*, 132470. [CrossRef]
108. Wang, Y.; Meng, Z.; Gong, X.; Jiang, C.; Zhang, C.; Xu, J.; Li, Y.; Bao, J.; Cui, Y.; Wang, H. Enhancing stability of Co$_9$S$_8$ by iron incorporation for oxygen evolution reaction and supercapacitor electrodes. *Chem. Eng. J.* **2022**, *431*, 133980. [CrossRef]